Chemical Engineering Journal 374 (2019) 155–169

Contents lists available at ScienceDirect

Chemical Engineering Journal

journal homepage: www.elsevier.com/locate/cej

Upgrading of zirconia membrane performance in removal of hazardous VOCs from water by surface functionalization

Joanna Kujawa[a,*], Wojciech Kujawski[a], Aleksandra Cyganiuk[a], Ludovic F. Dumée[b], Samer Al-Gharabli[c,*]

[a] Nicolaus Copernicus University in Toruń, Faculty of Chemistry, 7 Gagarina St., 87-100 Toruń, Poland
[b] Deakin University, Geelong, Institute for Frontier Materials, Waurn Ponds, Victoria 3216, Australia
[c] Pharmaceutical and Chemical Engineering Department, German-Jordanian University, Amman 11180, Jordan

HIGHLIGHTS

- Highly efficient zirconia membranes for hazardous VOCs removal process were generated.
- Improvement of transport properties after modification with fluorine-free molecules.
- Extensive material and physiochemical studies of functionalizes zirconia membranes.
- Correlation between physicochemistry and wetting properties of the modified ceramics.

ARTICLE INFO

Keywords:
VOCs removal
Zirconia ceramic membranes
Functionalization
Membrane distillation
Organic-inorganic separation materials

ABSTRACT

To upgrade the membrane separation process, there is a tremendous need to understand the process from the point of view of the membrane materials, e.g., their chemistry and material features. Functionalized by various alkyl- and fluoroalkylsilanes, zirconia membranes (pore size 3 and 200 nm) were systematically investigated from the material, physiochemical, and tribological points of view. The work shows the successful utilization of the modified ceramic membranes to niche application of water purification. Stable organic-inorganic membranes were applied in vacuum membrane distillation (VMD) for removal of hazardous volatile organic compounds (VOCs) butanol, methyl-*tert*-butyl ether, and ethyl acetate. Wettability, surface roughness, and adhesion were investigated, taking into account the type of modifiers (fluorine-free) and molecules with a different degree of fluorination. The impact of the type of reactive group in non-fluorinated modifiers on the material features and the separation effectiveness were discussed.

Furthermore, mechanical and chemical stabilities were studied. The most significant was that utilization of non-fluorinated modifier makes it possible to generate stable hydrophobic membranes, with high reactivity during grafting, suitable for VMD. These membranes possess better transport properties and high mechanical stability in comparison with fluorinated ones.

1. Introduction

The continuous increase of the human population on the earth which is accompanied by their basic and industrial activities has put a strain on the present sources of freshwater [1]. In a technically and economically feasible processes, water can be purified by the implementation of a variety of membrane separation processes including membrane distillation (MD) [1–3].

MD is an example of a non-isothermal process, demonstrates potential applications in various niche areas of scientific and industrial interest, especially, for the production of high purity permeate, recovery of valuable minerals, and separation of contaminants from liquid solutions [4,5]. Moreover, MD can be utilized to produce ultrapure water even from aqueous solutions with high salinity [6,7]. Considering all MD processes, vacuum MD (VMD) can be used for the removal of volatile organic compounds (VOCs) from industrial wastewater [8]. Furthermore, in the case of utilization membranes with high affinity to VOCs, the MD is an efficient and relatively low-cost process to remove

* Corresponding authors at: Nicolaus Copernicus University in Toruń, Faculty of Chemistry, 7 Gagarina St., 87-100 Toruń, Poland (J.Kujawa); Pharmaceutical and Chemical Engineering Department, German-Jordanian University, P.O. Box: 35247, Amman 11180, Jordan (S. Al-Gharabli).
E-mail addresses: joanna.kujawa@umk.pl (J. Kujawa), samer.gharabli@gju.edu.jo (S. Al-Gharabli).

https://doi.org/10.1016/j.cej.2019.05.160
Received 22 March 2019; Received in revised form 21 May 2019; Accepted 23 May 2019
Available online 24 May 2019
1385-8947/

VOCs. The mentioned feature gives MD the ability to apply low-grade waste heat to drive the process and make the it a promising green technology towards integrated zero liquid discharge purification processes [9]. Since the vapour pressure is not highly reliant on the salt concentration, MD can be coupled with reverse osmosis (RO) for the treatment of highly saline water [10] and upgrade the efficiency of the entire process.

VOCs due to their negative impact on the health and environment need to be removed from water. Beside their direct effect on the respiratory system, eyes, and skin, the presence of VOCs in water, even at low concentration, can introduce cytotoxicity, carcinogenicity, and autoimmunity [11]. Methyl *tert* butyl ether (MTBE), ethyl acetate (EtAc), and butanol (BuOH), are among the VOCs utilized on an industrial scale. Hazardous classification according to REACH for the above mentioned VOCs follows: H225 – highly flammable liquid and vapour; H226 – flammable liquid and vapour; H302 – harmful if swallowed; H315 – causes skin irritation; H318 – causes serious eye damage; H319 – causes serious eye irritation; H335 – may cause respiratory irritation, and H336 may cause drowsiness or dizziness [11]. There are number of separation techniques available and suitable to remove VOCs e.g. photocatalytic [12], adsorption [13], and catalytic combustion [14]. However, the reason to implement VMD instead of other techniques, presented above is high effectives of VOCs removal by membrane distillation. It needs to be highlighted that VOCs are good wetting agents for hydrophobic materials, and an application of conventional hydrophobic membranes (e.g. PTFE – polytetrafluoroethylene, PP -polypropylene) for MD is challenging. For this reason, a stable and highly efficient membrane material needs to be implemented. The separation materials dedicated to membrane distillation have to meet the following requirements: hydrophobic character, porous structure and lack of wetting during the separation process. To meet these necessities very often the modification of the materials is additionally introduced. A number of separation materials have been used for membrane distillation operation including polymeric and ceramic ones [7]. The first type due to the possible natural hydrophobicity is more popular. The other one, ceramic membranes, are generally more robust owing to their intrinsic properties, long-life, and high mechanical strength. Furthermore, ceramic membranes are less subject to fouling in comparison to polymeric membranes [15]. Unfortunately, ceramic membranes cannot be used for the MD process directly on account of their natural hydrophilic character [8,16]. Ceramic membranes must be hydrophobized prior to the application. This feature of the ceramic is actually beneficial due to the fact that properties of the material can be tune depend on the final application of the membranes. The membranes can be rendered hydrophobic by selective surface modification, such as the grafting of alkylsilanes and perfluoroalkylsilanes agents [17,18]. Furthermore, functionalization can be done in a way that membrane will be not wetted by the solvents, including highly concentrated VOCs in water. This is a predominance of ceramic membranes implemented in VOCs removal by MD in comparison with polymeric materials.

The most common ceramic materials used to date are titania, alumina, and silica substrate [2,6,18]. Titania and alumina are broadly used in the preparation of membranes with different geometry (planar, tubular [8,19], or hollow fibres [7]) for MD application [6,9,20–23]. On the other hand, zirconia shows interesting properties since it can improve material strength [24], possesses enhanced biocompatibility, and can be utilized in clinical applications [25]. Recently, more attention has been paid to the utilization of ZrO_2 in the MD owing to their lower thermal conductivity (2.1 $Wm^{-1}K^{-1}$) comparing to alumina (30 $Wm^{-1}K^{-1}$) and titania (11.8 $Wm^{-1}K^{-1}$) [26]. MD requires membrane materials with low thermal conductivity to prevent heat loss through the membrane. To date, such hydrophobized zirconia membranes have found very promising application in MD based desalination processes [27]. Liu et al. [28] presented hierarchically-structured ZrO_2 ceramic membranes prepared on the yttria-stabilized zirconia support. Significant enhancement of transport properties (high flux $-28.7\ kg\ m^{-2}h^{-1}$ and NaCl rejection coefficient > 99%) in MD was observed, which was related to the hierarchically organized mesopore structure. The ZrO_2 ceramic with the α-Al_2O_3 membrane was used by Wu at al. [29] to generate UiO-66-NH_2 membranes with high performance for the deep desulfurization of model gasoline via the pervaporation process. Zhang et al. [30] compare two types of polymeric membrane modules in the removal of VOCs from wastewater implementing VMD. The synthetic feed contained 1 wt% sodium chloride and 2.2 wt% VOCs (dimethoxymethane, formaldehyde, and methanol at a mass ratio of 10:2:1) based on an industrial wastewater composition. Authors observed wetting of the membrane and suggested an additional modification of the membrane to avoid the tat problem.

Taking into account advantages of zirconia material (i.e. thermal conductivity, high mechanical stability and biocompatibility as well as the cost of the raw material) and their potential in the VOCs removal by MD it was possible to define the research gaps. Namely, there are lack of references focusing on the utilization of ZrO_2 based membranes for VOCs removal. Bearing in mind the potential applicability of these membranes in water treatment, the environmentally friendly separation materials are desired. To meet the mentioned expectations, the authors proposed the utilization of zirconia ceramic membranes functionalized by non-fluorinated grafting agents.

The aim of the presented work is the base research focused on the grafting of zirconia ceramic membranes and assessment of their efficacy in a VMD process applied for the removal of VOCs. The membranes were furnished with alkyl-chains possessing varied degrees of fluorination and anchoring roots, i.e. chlorine, ethoxy and methoxy groups. An important part was to correlate and to discuss the wettability and roughness of the functionalized ceramic materials. The new materials were characterized, and the separation efficiency was correlated with the surface energy and wettability of the materials. This strategy opens up new avenues for fabrication ceramic, highly stable and resistant materials for water purification from hazardous volatile organic compounds address to niche and advanced application.

2. Experimental part

2.1. Materials

Tubular (single-channel) ceramic ZrO_2 membranes with a molecular-weight-cut-off (MWCO) equal to 5kD (~3 nm pore size) and 300kD (~200 nm pore size) were purchased from TAMI (France). For material characterization, planar zirconia membranes with 3 and 200 nm pore size were utilized. 1H,1H,2H,2H-perfluorooctyltriethoxysilane (CAS 51851-37-7) marked hereafter as **FC6**; 1H,1H,2H,2H-perfluorodecyltriethoxysilane (CAS 101947-16-4) marked hereafter as **FC8**; 1H,1H,2H,2H-perfluorododecyltriethoxysilane (CAS 146090-84-8) marked hereafter as **FC10**; and 1H,1H,2H,2H-perfluorotetradecyltriethoxysilane (CAS 885275-56-9) marked hereafter as **FC12** were selected as the grafting agents (SynquestLab, USA) containing fluorine atoms. Moreover, fluorine-free molecules: n-octyltriethoxysilane (CAS 2943-75-1) referred hereafter as **C6OEt**, octyltrimethoxysilane (CAS 3069-40-7) referred hereafter as **C6OMe**, and octyltrichlorosilane (CAS 5283-66-9) referred hereafter as **C6Cl** were purchased from Abcr Chemicals GmbH (Germany). The grafting process and preparation of the modifying solutions were done and kept under argon to avoid self-condensation. BuOH, MTBE, and EtAc were chosen as examples of hazardous VOCs. Acetone, butyl acetate, chloroform (stabilized by 1% ethanol), dimethyl sulfoxide, ethanol, ethyl iodide, glycerine, n-hexane, perfluorohexane, and pyridine were used for the critical surface tension (γ_{cr}) determination. All the above-mentioned solvents were purchased from Avantor Performance Materials Poland S.A (Poland) and used without further purification. RO deionized water (18 MΩ.cm) was used for the preparation of model VOCs aqueous solutions utilized during VMD.

2.2. Methodology

2.2.1. Material features of native and hydrophobized ceramic membranes

Based on the goniometric technique (goniometer Attention Theta - Biolin Scientific, Gothenburg, Sweden), apparent contact angle (CA) and CA hysteresis (HCA) were determined. The tilting plate method was applied at room temperature with 5 s of equilibration [31]. The presented values of CA were the averaged values from 20 to 30 individual measurements. The wettability limits expressed by γ_{cr} were determined based on the Zisman method [32]. The surface free energy (SFE) was calculated based on the Owens, Wendt, Rabel, and Kaelble (OWRK) method [33]. The pore size distribution and pore size of the ceramic materials were determined to implement BET (Brunauer–-Emmett–Teller) [34,35] and BJH (Barrett-Joyner-Halenda) [34,35] models (Nitrogen adsorption/desorption analysis ASAP 20120 Micromeritics Instrument Corp., USA). Directly before the pore size determination, ceramic samples were degassed at 90 °C for 2 h. The roughness parameters of the membranes were assessed at room temperature by atomic force microscopy (AFM) (NanoScope MultiMode SPM System and NanoScope IIIa and Quadrex controller, Veeco, Digital Instrument, UK) employing the tip scanning mode with silicon nitride probes (NP-1, Veeco) ($k = 0.58\ Nm^{-1}$) and a scanning area of the samples equal to 5 μm × 5 μm. Roughness was presented as a root mean square (RMS) achieved from NanoScope Analysis Software (1.40, Build R3Sr5.96909, 2013 Bruker Corporation). Contact mode with a diamond probe (DNISP-HS, Bruker) ($k = 600\ Nm^{-1}$) was utilized during tribological measurements. Adhesive forces (F_{adh}), nanohardness (H), and Young modulus (E) were selected as parameters related to the tribological features [8]. In the case of E and H determination, measurements were repeated six times. Presented final values of F_{adh} were averaged from thirty analyses.

The effectiveness of the hydrophobization process was assessed by the goniometric method and by liquid entry pressure (LEP_w) determination (tubular membranes) (Eq. (1)). Prior to the LEP_w measurements, hydraulic permeability measurements (L_p) were performed (Eq. (2)). The L_p was achieved using a laboratory rig [36]. The permeability of all non-modified membranes was evaluated by a linear regression of water flux applying an increasing of transmembrane pressure in the range of 1–9 bar (Eq. (2)).

$$LEP_w = \frac{2\gamma_L}{r_{max}} cos\theta_{ef} \tag{1}$$

$$J_v = L_p \Delta p \tag{2}$$

where γ_L – surface tension of the applied testing liquid, r_{max} – maximum membrane pore size, and θ_{ef} – effective contact angle value, J_v – water flux, Δp – transmembrane pressure.

2.2.1.1. Membrane grafting process. The hydrophobization process of ceramic membranes (planar and tubular) was accomplished based on the previously developed protocol [8,37]. The modification process of the ceramic samples is presented in Fig. 1. The pre-treated (cleaned and dried) membranes were grafted by submerging a sample in a grafting solution (0.05 M). Modifiers were from a group of fluorinated (FC6OEt, FC8OEt, FC10OEt, FC12OEt) or non-fluorinated (C6OEt, C6OMe, C6Cl) compounds. All the samples were kept in a grafting solution under argon atmosphere for 15 h at room temperature. Once the functionalization process was accomplished, the ceramics were taken out from the solution of grafting agent and consecutively rinsed in pure ethanol, acetone, and water. Finally, membranes were dried at 90 °C overnight and stored in the air.

The effectiveness of the grafting was assessed by TGA, NMR and FTIR. Attenuated total reflection–Fourier transform infrared spectra (ATR-FTIR) were collected using Bruker Vertex 80v ATR-FTIR machine (256 scans, $4\ cm^{-1}$ resolution). Solid-state cross-polarization/magic angle spinning nuclear magnetic resonance (CP/MAS NMR) measurements (^{29}Si) were done on Bruker Avance 700 MHz. Hydroxyl groups determination on pristine and modified materials was performed implementing thermoanalyzer Jupiter STA 449 F5 (Netzsch, Germany). TGA analyses were accomplished at the temperature range of 25–1000 °C under an ambient atmosphere of nitrogen.

2.2.1.2. Vacuum membrane distillation (VMD). The modified tubular zirconia membranes were tested in VMD processes for the removal of hazardous VOCs. Membranes, after the hydrophobization process were pretreated (conditioning step) by keeping in contact with pure water during the MD process until the constant flux had been reached (usually after 5–7 h) [37]. This part was necessary to remove all non-covalently attached silanes molecules that were anchored only by the physical interactions (e.g. adsorption) on the membrane surface or inside the pores [37]. Prior to the VOCs removal, values of permeate fluxes for pure water as a feed were determined. The VMD tests were done at 35 °C, applying the setup shown and described in detail elsewhere [37]. Butanol, ethyl acetate, and methyl-*tert*-butyl ether were selected as hazardous VOCs to prepare the model aqueous solutions, containing 3 wt% of VOCs. The separation properties of the tested membranes were determined based on the GC analyses of the feed and permeate composition. Varian 3300 apparatus with a thermal conductivity detector (TCD), and PorapakQ packed column (injection port temperature at 200 °C, detector temperature at 220 °C and column temperature at 180 °C) was used.

The efficacy of the VMD experiments was evaluated by using the following factors – total flux (J) – Eq. (3), partial permeation fluxes (J_1) – Eq. (4), separation factor (β) – Eq. (5), and Process Separation Index (PSI) – Eq. (6) [19].

$$J = \frac{\Delta m_t}{\Delta t \cdot A}\ [kg \cdot h^{-1} \cdot m^{-2}] \tag{3}$$

$$J_1 = J \cdot Y_1\ [kg \cdot h^{-1} \cdot m^{-2}] \tag{4}$$

$$\beta = \frac{Y_p}{X_p} \cdot \frac{X_f}{Y_f} [-] \tag{5}$$

$$PSI = J(\beta - 1)\ [kg \cdot h^{-1} \cdot m^{-2}] \tag{6}$$

where Δm_t – total weight of the compound in permeate [kg], A – an area of the membrane [m^2], Δt – a time of permeation [h], Y, X – mass fractions of the more permeable component in permeate and feed, respectively.

2.2.1.3. Evaluation of hydrophobic layer stability. The mechanical and chemical stabilities of the modified membranes were also assessed. The chemical stability was evaluated by putting the hydrophobized membranes in contact with the following pure solvents: acetone, butanol, chloroform, ethyl acetate, hexane, and methyl-*tert*-butyl ether. The membranes were immersed in pure solvents for 96 h. The solvent was stirred, providing a constant tangential flow over the membrane surface. Subsequently, the membrane was rinsed with deionized water and kept overnight at 90 °C. The mechanical stability was determined by keeping samples in a sonication bath for 4 h, followed by membrane cleaning in ethanol, acetone, and water, and drying the sample at 90 °C overnight. Assessment of thermal and mechanical stabilities was evaluated using the goniometric method. Additionally, to evaluate influence of presented treatment by chemicals or sonication, the transport and separation features for the treated membranes were also determined. The purpose was to show if any impact on membrane performance could occurred due to the contact with chemicals or ultrasounds.

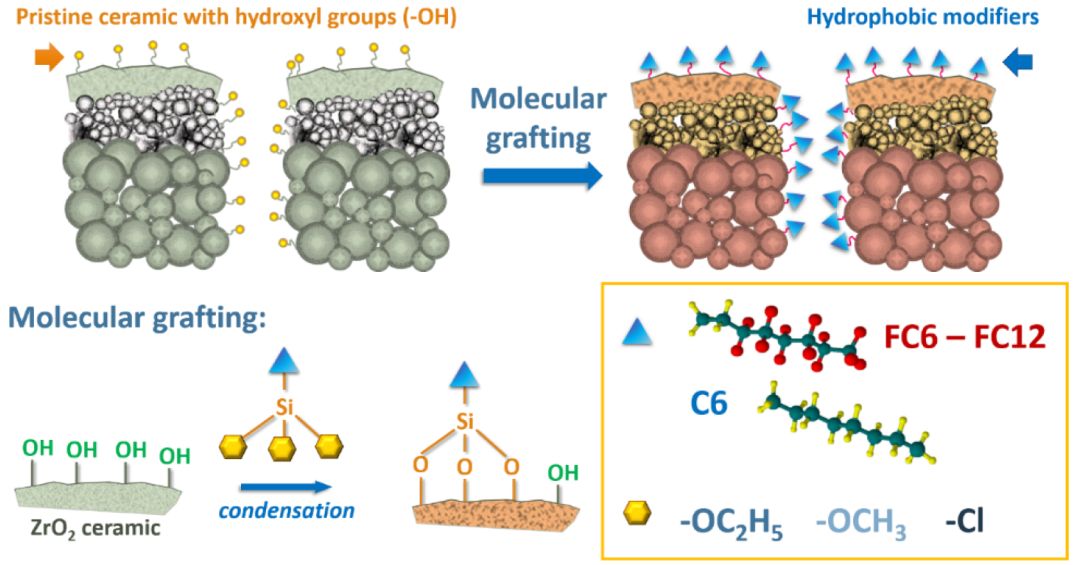

Fig. 1. The scheme of ceramic membranes functionalization by tri-functional perfluoroalkylsilanes molecules.

3. Results and discussion

3.1. Pristine ceramic membranes

Pristine zirconia membranes have been systematically examined by the set of analytical methods. Goniometric measurements were done with planar samples. In the description of the materials designed for the membrane distillation, the crucial is a wettability of the material. Therefore, a detailed evaluation of water behaviour for pristine and hydrophobized samples was performed. Based on the Eq. (7) and dynamic contact angle measurements, water penetration profile into the ZrO_2 ceramic structure was calculated (Fig. 2B) [38].

$$\chi = \sqrt{\frac{d_p \cdot \gamma_{LV} \cdot t \cdot \cos\theta}{4\eta}}\ [m] \tag{7}$$

where χ – depth of liquid penetration [m]; d_p – pore size [m]; γ_{LV} – liquid vapor surface tension [mN m^{-1}]; Θ– contact angle [deg]; t – time [s]; η – solvent viscosity [Pa s].

$$S = W_{1,2} - W_{1,1} \tag{8}$$

Another calculated parameter was a spreading pressure (S) (Eq. (8)) [39,40], being a difference of adhesion work between the phases and cohesion work of the phase under consideration (testing liquid). The determined value of S can be either negative (incomplete wetting) or positive (liquid penetration into the material) [39,40]. Because of spreading pressure is directly related to the surface tension of the material, the same values equal to -17.03 ± 0.56 mN m^{-1} were found for 3 and 200 nm samples.

Although the same hydrophilic character (CA ~ 40°) was observed for the 3 and 200 nm membranes (Fig. 2A), water molecules behave differently depending on the pore size. A 3 nm membrane possessing a more dense structure and lower porosity (ca. 32%) was characterized by a shorter time of liquid penetration into the ceramic structure. Practically only soaking to the material was observed (Fig. 2B). In the case of the 200 nm sample (porosity ca. 40%), faster water penetration,

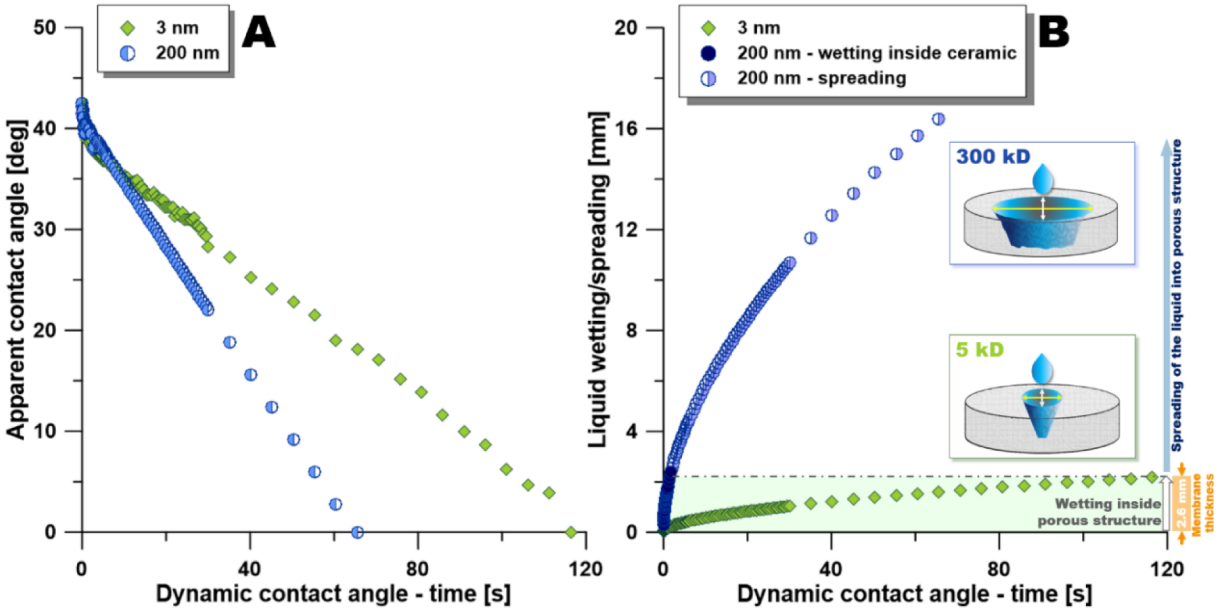

Fig. 2. A – Apparent contact angle evolution in the course of measurement, B – Liquid wetting/spreading – the depth of water penetration into the ceramic structure of 3 nm and 200 nm membranes.

and the additional effect of water spreading was observed (Fig. 2B). After 120 s, water penetration approached 82% of membrane thickness (2.13 mm, total membrane thickness = 2.6 mm) (Fig. 2B), the CA after that time was around 3° (Fig. 2A). The water penetration was related to the normal presence of capillary forces. For the 200 nm sample, the testing liquid spread onto the porous structure in the directions presented in Fig. 2A. Based on Eq. (7), the time necessary to soak/spread into the materials was 40 s.

Although the water was chosen as a testing liquid (no impact of the concentration), the speed of water penetration into the ceramic ZrO_2 support can be defined by zero-order kinetics. Determined constant rate (k^0) for penetration/soaking of water was equal to 0.327 and 0.594 mol dm^{-3} s^{-1} for the 3 and 200 nm pore size ZrO_2 ceramic non-modified membranes, respectively. For both samples of 3 and 200 nm, the same value of surface free energy, equal to 141 ± 3 mN m^{-1}, has been observed. Critical surface tension (γ_{cr}) influences the membrane applicability and solvent selection for cleaning. Application of solvents with a lower γ_L than γ_{cr} of a membrane will wet the membrane material. The calculated values of γ_{cr} for the 3 and 200 nm ZrO_2 samples were equal to 28.1 ± 1.2 mN m^{-1} and 35.6 ± 1.5 mN m^{-1} m^{-1}, respectively.

The difference in membrane morphology is related to the dissimilar pore size as well as roughness parameters (RMS). The more open structure shows higher RMS values of 59.3 ± 1.6 nm for the 200 nm sample compared to 43.2 ± 1.3 nm for 3 nm membranes. The variations in porous structure also impacted the mechanical properties, expressed by tribological parameters. F_{adh}, E, and H determined based on AFM measurements were 25.21 ± 0.82 nm, 118.3 ± 2.41 GPa, and 4.85 ± 0.12 GPa for the 3 nm ZrO_2 membrane, respectively. 200 nm ZrO_2 material has been characterized by 29.47 ± 0.77 nm, 111.4 ± 2.22 GPa and 4.33 ± 0.11 GPa.

An important factor was the amount of hydroxyl groups available first on the pristine material and then on the modified one. The differences of these two factors defined packing density of the grafting (Eqs. S1 and S2). The hydroxyl groups were determined by TGA and NMR method descript in details elsewhere [41].

Pristine ceramic membranes of tubular-geometry were characterized by a hydraulic permeability determined on the basis of Eqs. (1) and (2). The 3 and 200 nm ceramic membranes were characterized by the L_p (Eq. (1)) equal to 0.21 × 10^3 kg h^{-1} m^{-2} bar^{-1} and 2.15 × 10^3 kg h^{-1} m^{-2} bar^{-1}, respectively. The observed differences are associated with the morphology of the membrane (pore size, porosity, and tortuosity).

3.2. Hydrophobized ceramic membranes

In the first step, the membranes were examined by SEM technique (Figs. S1 and S2) to face any differences related to the modification (Fig. S3). The adsorption-desorption nitrogen isotherms, BET and BJH models [35,42] were implemented for the evaluation of the grafting process on the pore size (Fig. 3). The hydrophobization effectiveness has been assessed by determination of C parameters (Eqs. (9) and (10)) expressing the adsorption equilibrium and degree of interaction between adsorbent and adsorbate.

$$a = \frac{a_m C \frac{p}{p_0}}{\left(1 - \frac{p}{p_0}\right)\left[1 + (C-1)\frac{p}{p_0}\right]} \quad (9)$$

$$C = exp\left(\frac{E_1 - E_L}{RT_a}\right) \quad (10)$$

where a – total volume of adsorbed gas at p pressure, p_0 – adsorbates saturation pressure at the temperature of adsorption, p - adsorbates equilibrium pressure at the temperature of adsorption, a_m – monolayer capacity (volume of gas adsorbed by monolayer), C – BET adsorption equilibrium constant, E_1 – adsorption heat for the first layer, E_L – adsorption heat for the second and higher layers for which the value is equal to the heat of liquefaction.

The value of C parameter depends on the chemistry of the sample, particularly on the amount of surface uncovered by adsorbate when sufficient adsorption occurred in monolayer, and it is varying on the substrate [42,43]. Pore size, surface porosity, and capacity of adsorption [34,35] have also impact on C. The established C parameter for ZrO_2 were equal to 58.35 and 8.25. The higher value of C found for the 200 nm membrane can be related to the higher ability to adsorb, the higher number of available hydroxyl groups on the raw material as well as more open structure (Fig. 3), making it possible to attach modifiers easily inside the membrane pore size [43]. The concentration of available hydroxyl groups was determined according to the developed method and presented in Fig. S4. The noticeable difference between utilization of hydroxyl groups and then loading of fluorinated and non-fluorinated modifiers has been observed (Fig. S4.A). Higher efficacy was observed for the non-fluorine modifiers. In the case of fluorinated modifiers, the efficiency was in the range of 48% (FC10) and 64% (FC12). On the other hand, fluorine free modification was characterized by the yield of 75% (C6OEt) and 91% (C6Cl) (Fig. S4.A). The reduction of C parameter in comparison to the non-modified ceramics is a result of the modification, a decrease in surface areas and the reduction of pore size (Fig. 3B). Comparing the isotherms for pristine (NM) and modified samples, it can be seen that the shape of the isotherms is different. In the case of samples hydrophobized by FC6 and C6OEt the registered isotherms are characteristic for porous material with cylindrical pores possessing various cross-sections [44]. On the other hand, isotherms for membranes grafted with more hydrophobic molecules (FC12) were characteristic for materials with spherical pores possessing moreover a lot of narrowings [35,42]. The hydrophobicity level of the grafting agent had an important impact on the size and presence of a hysteresis loop. A smaller hysteresis loop has been observed for the surface modified by molecules with longer alkylsilane chains. Comparing the same length-molecules, the presence of fluorine contributed to the enlargement of the hysteresis loop (Fig. 3A). The presented variations were related to the alterations in membrane morphology, i.e. pores tortuosity. It can be confirmed by the reduction in the value of the C parameter (Fig. 3B) [34,35,42]. The presented tendency has been found for both 3 and 200 nm membranes. The values of the C parameter were equal to 22.6 and 58.4 for pristine samples, for the 3 and200 nm, respectively. The significant reduction of the C factor for the modified 200 nm membranes was related to the hydrophobization of the entire porous volume. An interesting observation was related to the slight impact of the type of reactive group on the adsorption capacity (Fig. 3B). As can be observed, the surface functionalized with C6Cl possessed the lowest value of the C parameters causing the lowest adsorption (Fig. 3B).

3.3. Material properties of functionalized membranes

3.3.1. Ceramic membranes with planar geometry

Four types of perfluorinated molecules (FC6, FC8, FC10, and FC12) and three non-fluorinated (C6OEt, C6OMe, and C6Cl) compounds were selected as grafting agents. The reason for choosing non-fluorinated modifiers was to investigate the impact of the type of reactive group on the efficacy of modification and membrane properties as well as to compare the presence or absence of fluorine atoms (i.e. for molecules possessing the same reactive group and length).

Basing our findings (Figs. 4 and 5), it can be concluded that the type of grafting agent and pore size have an important impact on the wettability and roughness. Pristine samples were characterized by the apparent CA of ca. 40° (Fig. 2). On the other hand, after modification, membrane surfaces changed from hydrophilic to hydrophobic with CA above 120° (Fig. 4). The observed effect has been presented by different groups [1,18,24,45]. The most used compounds for the modification of ceramic were 1H,1H,2H,2H-perfluorooctyltriethoxysilane,

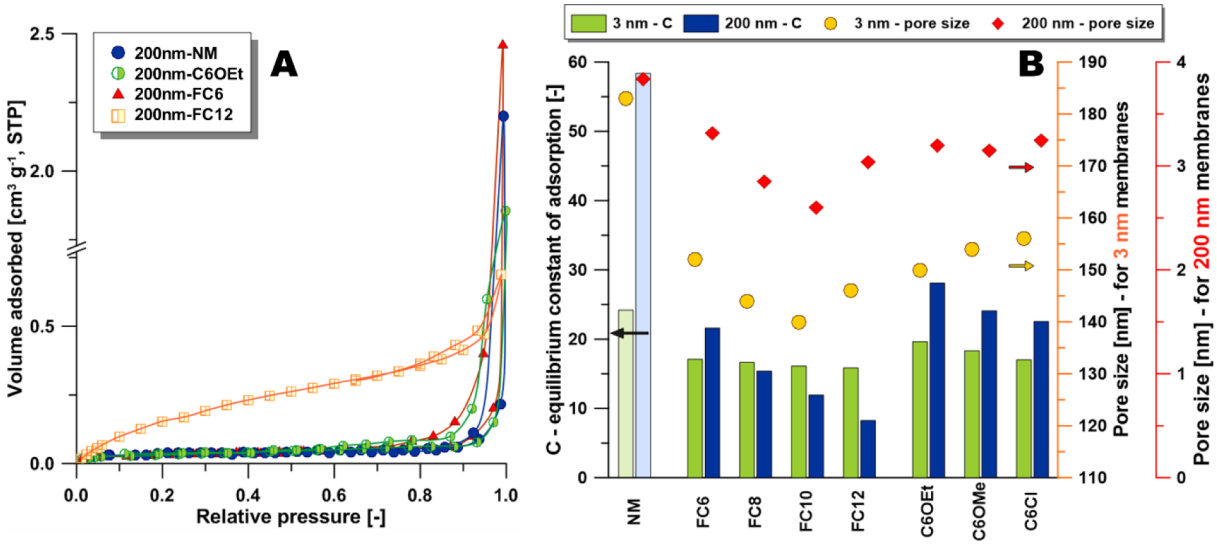

Fig. 3. A – Nitrogen adsorption-desorption isotherm of 200 nm non-modified (NM) and functionalized membranes by non-fluorinated C6OEt and perfluorinated FC6 and FC12 compounds; B and C parameter for pristine (NM) and functionalized 3 nm and 200 nm membranes.

1H,1H,2H,2H-perflourodecyltriethoxysilane [1,24,45], and 1H,1H,2H,2H-perfluorooctyltrichlorosilane [18]. These modifiers have also a broad range of application in hydrophobization of different substrate e.g. cotton, wood, zeolites [18,45].

Membranes modified with fluorinated molecules show a highly hydrophobic surface with CA up to 135° in the case of the 200 nm membranes. Surprisingly, samples hydrophobized with FC10 were characterized by a lower value of CA compared to the other fluorinated molecules (Fig. 4A). This fact was related to a higher reduction in the pore size of the membrane (Fig. 3B). Furthermore, it has a strong impact on the water resistance as well as causing an increase in critical surface tension for ceramics modified with FC10 (Fig. 4B). This behaviour was reported in our previous work and was explained by the implementation of ^{29}Si NMR technique [8]. It was mentioned that FC10 molecules could form tangled chains and subsequently, generate a more rough surface [8]. Such odd results can be also explained by the presence of traces of water (i.e., the equilibrium of adsorbed surface water film) [46] that can promote the hydrolysis of reactive groups (OEt, OMe, and Cl) to silanol intermediates. As a result, bulk vertical polymerization can take place, significant in the generation of disordered silanes clusters and finally increasing surface roughness and decreasing packing density. Indeed, the higher roughness for samples grafted with FC10 was also observed in the presented study (Fig. 4B) which can be linked to the lower density of active groups on the ceramics and therefore a reduced grafting density and a higher degree of polysiloxane polymerization. Furthermore, these variations can be introduced by different grafting mechanism. The differences in the mechanism of grafting modification (mode of modifiers attachment) has been first study by ^{29}Si MAS-NMR and subsequently taken into account in the grafting loading determination (Fig. S4.B). Similarities in the mode of molecules attachment were noticed for non-fluorinated agent. These molecules were mostly attached by 1 (T^1) and 2 (T^2) reactive groups. The contribution of T^3 type of bonds by 3 reactive groups were in the range of 19–29%. For fluorinated modifiers FC6, FC8 and FC12 similarities have been found. The overall lower loading of the grafting molecules in the comparison to fluorine-free modifiers was related to the different conformation. However, substantial difference was observed for the modification with FC10. In this latter case, the modifier molecules were attached mostly by the T^3 connections. Taking into account the highest space consumption on the surface of zirconia ceramic support by attachment mode with 3 reactive groups and high length of the modifier, grafting with FC10 was characterized by the lowest grafting effectiveness.

The roughness of the fluorinated membranes was reduced as a

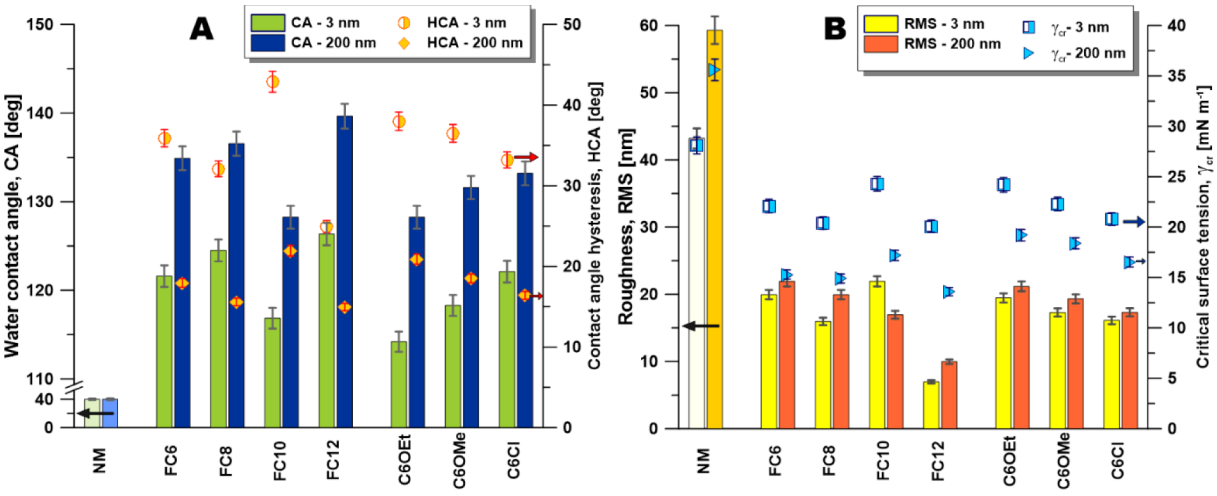

Fig. 4. A – Wettability behaviour – contact angle and hysteresis of CA; B – surface roughness and critical surface tension (γ_{cr}).

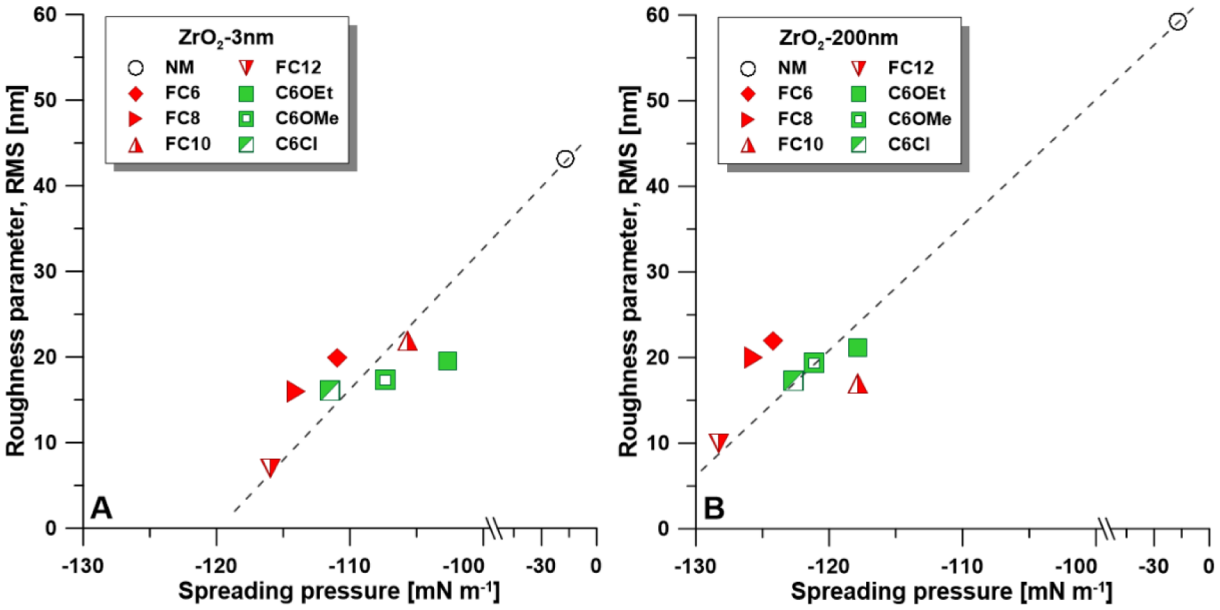

Fig. 5. Correlation between surface roughness and spreading pressure.

function of fluorination, and the application molecules with longer fluoroalkyl chains, with one exception for the FC10 in the case of the 3 nm sample. Measurements show the roughness of 43.2 ± 1.5 nm, 59.3 ± 1.3 nm for the 3 and 200 nm pore size membranes respectively, in comparison with the lowest values 6.98 ± 1.1 nm and 9.97 ± 1.2 nm achieved for FC12 modification of 3 and 200 nm pore size membranes, respectively. The RMS of the non-fluorinated membranes ($RMS_{3nm\text{-}C6OEt}$ = 19.5 ± 1.5 nm; $RMS_{200nm\text{-}C6OEt}$ = 21.2 ± 1.3 nm) were comparable to the fluorinated analogue possessing the same length and functional group of the alkyl chain ($RMS_{3nm\text{-}FC6}$ = 19.9 ± 1.3 nm; $RMS_{200nm\text{-}FC6}$ = 21.9 ± 1.3 nm). Higher values of CA for membranes with bigger pores was related to the higher roughness of this type of surfaces (Fig. 4B). In the case of water presence, the formation of covalently bonded monolayers is favored, which can form horizontal siloxane networks causing self-assembly [46]. Limited impact of the reactive group on the membrane heterogeneity was demonstrated. The most inert groups were etoxy- and methoxy-ones, whereas chloro-silane was the most labile one. The above mentioned factors impacting the interaction between vertical and horizontal polymerization of the silanols were not certainly correlated to the length of the grafting molecules. A longer chain of perfluorinated molecules should offer better molecular organization and generate a smoother coated layer. Conversely, the hindrance-steric-effect of longer chains may probably restrict crosslinking in the horizontal direction and closely packing molecules during the modification process, increasing roughness. Furthermore, grafting molecule volatility as well as the availability of monomers declines with an increase in molecule length that may causeless less molecular packing during the coating process [46,47].

CA is a complex parameter on which chemistry and material morphology have an important influence. A number of material properties, e.g., roughness, wettability, physiochemistry (surface free energy) have a significant influence on the final CA value. In the case of membranes modified by non-fluorinated molecules, an interesting impact of the reactive group type was observed. The sample modified with C6Cl was characterized by high effectiveness expressed by the highest CA and the lowest hysteresis of CA. Conversely, the lowest hydrophobicity was observed for C6OEt. This finding needs to be correlated with the energy of bonds dissociation, the highest being for -Si-Cl [8]. Considering non-fluorinated membranes, a slightly lower hydrophobic character was reached, by ca. 5% (Fig. 4A). It is related to the larger radius of perfluorinated (5.90 Å) chains compared to fluorine-free (4.97 Å) analogues. Variations in the size of the molecule cause the higher value of the energy penalty for hydration [48]. To explain the presented differences of higher CA for fluorinated samples, the chemistry of the modified surface needs to be considered. Namely, the hydration free energy on the hydrophobic surface unit is similar for fluorocarbons and hydrocarbons [48]. Carbon-hydrogen bonds are characterized by a smaller value of dipole moment comparing to C-F. Therefore, weaker interaction with dipolar molecules of water could be predicted, considering the low polarizability of fluorine atoms in −C−F bond. In contrast, the hydration-free energy of C−H is equivalent [49], and interactions of dispersion for C−H bonds with molecules of water will be feasibly less attractive than for C-F. For that reason, a membrane modified with fluorine-free modifiers can possess even lower hydrophobicity than fluorinated samples [48]. Nevertheless, owing to the bigger lattice spacing of perfluoroalkylsilanes molecules, fluorinated surfaces will be characterized by a higher hydrophobicity level [48].

Based on the collected data (Fig. 4A), it can be stated that a diminution of HCA is directly related to the increase in the hydrophobicity level by the application of perfluoroalkylsilanes with longer fluoro-carbon chains or molecules with more reactive groups, i.e., −Cl. However, the presence of fluorine, when the same-length molecules were shown, possessed a negligible impact. The value of HCA for 3 nm membranes modified with FC6 and the set of non-fluorinated agents were in the range of 33.2 ± 1.0°–38.0 ± 1.0° (between C6OEt and C6Cl) and for fluorinated ones were equal to 35.9 ± 1.0°. The lowest value was measured for FC12 sample 24.9 ± 1.0° (Fig. 4A). More relevant differences were found on the surface of the 200 nm membranes. Additionally, the values of HCA were smaller for the 200 nm samples in comparison to the 3 nm. Fluorine-free surfaces were characterized by HCA between 16.4 ± 1.0° (C6Cl) and 20.9 ± 1.0° (C6OEt). HCA for fluorine-rich membranes was in the range of 14.9 ± 1.0° (FC12) and 21.9 ± 1.0° (FC10) (Fig. 4).

Wettability was evaluated comprehensively, determining critical surface tension γ_{cr} (Fig. 4) and spreading pressure S (Fig. 5). As an effect of the modification, a reduction of the critical surface has been observed to 13.6 mN m^{-1} (200 nm-FC12). In the case of 3 nm membranes, a reduction in the range of 21.4% and 28.5% for fluorinated compounds was observed. A more significant reduction between 57.1% (FC6) –61.8% (FC12) was found for the 200 nm membranes, especially for surfaces treated with perfluoroalkylsilanes (Fig. 4B). Generation of the

surfaces possessing lower values of the critical surface tension has an essential meaning from the application point of view. Specifically, such surfaces with as low as possible γ_{cr} will be characterized by excellent resistance to wetting. The value of γ_L for salty water used in the desalination process by MD is around 79.1 mN m^{-1} [50], so ensuring the lack of wetting during the separation process with prepared membranes, possessing the γ_{cr} in the range of 24.3 mN m^{-1} (3 nm-FC10) and 13.6 mN m^{-1} (200 nm-FC12) (Fig. 4). This feature of the material is extremely important in the formation of the membranes dedicated to the membrane distillation process to meet one of the most important requirements addressed to MD materials [15]. Lastly, it was possible to form surfaces with a higher hydrophobicity level implementing the molecules with shorter perfluoroalkyl chains, e.g., FC6 instead of FC8 or FC10, independently from the selected membranes. It was likely to perform hydrophobic sampling by functionalization with a fluorine-free modifier. The highest reactivity of modifier with -Cl was related to their low value of the bonds dissociation (Si-Cl) equal to 253 kJ mol^{-1} compared to Si-O(Me/Et) equal to 452 kJ mol^{-1} [51].

Spreading pressure (S) provides an insight into the wetting behaviour of membranes. An established S parameter was characterized by negative values and nonzero CA for all tested membranes, before and after the hydrophobization process (Fig. 5) [52]. The calculated values of S were in the range of -17.03 ± 0.56 mN m^{-1} (NM) to -128.28 ± 4.2 mN m^{-1} (200 nm-FC12. The negative value of S is a common phenomenon for a material with a high hydrophobicity [52]. The lower value of the S parameter for the more hydrophobic sample (C6OEt and FC6) is referred to smaller basicity of the sample. In Fig. 5 the correlation between spreading pressure and roughness is additionally plotted. An interesting correlation has been observed. The linear relation between S and RMS for membranes treated with non-fluorinated molecules was observed, proving the mentioned relation between the reactivity of the head groups and the effectiveness of the coating process.

The surface free energy (overall value, dispersive, and polar components) (Fig. 6) is another parameter that was selected for the material characterization of ceramics. Owing to the formation of highly hydrophobic surfaces, a significant diminution of the SFE was found. A low value of the polar part was observed. For the non-modified surfaces, the values of the polar part are around 40% of overall SFE. As an effect of the modification, a reduction to ca. 14–22% of the initial value was observed. Moreover, the modification revealed the variation in the SFE, taking into account the pore size of the samples (Fig. 6). In the case of pristine samples, no impact of the surface heterogeneity has been found. Considering ceramic membranes functionalized with the set of fluorinated molecules, the highest values were determined for surfaces (3 nm and 200 nm) grafted by FC10 (overall $SFE_{3nm\text{-}FC10} = 33.12 \pm 1.32$ mN m^{-1}, $SFE_{200nm\text{-}FC10} = 33.12 \pm 1.32$ mN m^{-1}). Depending on the reactive group, the total SFE value was in the range of 31.50–34.75 mN m^{-1} for the 3 nm and in the range of 19.88–23.81 mN m^{-1} for the 200 nm, respectively. However, a much smaller contribution of the polar component was found for 200 nm, ca. 15% of total SFE. In the case of the 3 nm, that factor was above 20% (Fig. 6). The established results are in good accordance with the literature [47].

Thermodynamically, the wettability behaviour of the solid surface can be defined, taking into account free energy related to the generation and elimination of interfacial areas. The formation, as well as the destruction of interfaces, entails changes in reversible free energy expressed as an equilibrium adhesion work [46,53]. The adhesive force acting in an ambient environment between the solid substrate (i.e., ceramic) and AFM tip is usually reported to originate predominantly from distortion and destruction of the capillary bridges between tip and surface [46,53]. Very often such bridges originate from the condensates of water vapours which accidentally form at structural irregularities, e.g., pores or cracks. The corrugation of the surface at various scales, e.g., nano or micro, may allow water to penetrate across the mentioned irregularities and finally generate nano- or micro-droplets, even on the hydrophobic or highly hydrophobic surfaces [46,54]. Such behaviour has been found for all investigated ceramic samples coated with perfluorinated and fluorine-free molecules, showing the RMS values in the range of 6.9–21.9 nm.

Taking into account the capillary forces, having a nature independent of the chemistry of surface structure, an important impact on the measured adhesive force can be observed. However, the mentioned parameter is not the only one affecting F_{adh}. However, the data shown in Fig. 6A suggest that increasing the number of carbon atoms in the grafting agent caused a significant reduction of adhesion forces. In the case of capillary condensation, the determined F_{adh} might be sensitive to the chemical specificity of the surface (i.e., the length of molecules, the presence of fluorine and/or type of reactive group). In the presented case, both dispersive and capillary interactions can contribute to the F_{adh} value (Fig. 6). Practically a linear relation has been found between F_{adh} and SFE values. Moreover, in the case of a polar component of SFE, the value of F_{adh} corresponds to a very small range of that SFE part equal to 1.7 mN m^{-1} and 1.6 mN m^{-1}, for 3 nm and 200 nm, respectively (Fig. 6A1, A2). In the case of the 3 nm samples, the relation is approximately linear, except for the samples grafted with FC10 (Fig. 6A1). On the other hand, for the 200 nm ceramics (Fig. 6A2) such an exception was found for FC6 coating. The presented features are related to the fact that for the longer chains (i.e., FC10) a predominant contribution of the dispersive part is associated with a smaller value of the capillary component of F_{adh}. Interestingly, the big difference in the data point's location in Fig. 6A1 and A2 of polar components were observed for membranes treated with FC10. That statement indicates the low packing density and an extensive horizontal polymerization, resulting in a higher contribution of the polar part and explaining higher roughness (Figs. 4 and 5). In Fig. 6B, the local adhesive features are shown by presenting a comparison of F_{adh} with the microscopic work of water-ceramic system adhesion. The substantial drop of F_{adh} and work of adhesion has been noted with an increase of the length of the grafting (excluding FC10 coating) agents and with the reactivity of terminal groups.

3.3.2. Tubular ceramic membranes

Owing to the limitation of analytical techniques for analyzing tubular-geometry samples, only liquid entry pressure values (Eqs. (1) and (2)) were determined to assess the efficiency of membranes modification. For non-modified samples, for both 3 and 200 nm pore size membranes, the first drops of water appeared directly during the LEPw measurement without applied higher pressure difference. The observed phenomenon can be explained by water penetration into the hydrophilic structure of ceramics under practical lack of pressure difference. After treatment with fluorinated and fluorine-free molecules, an increase of LEPw was observed up to a maximum of 0.40 MPa. The lowest value of LEPw equal to 0.25 MPa was found for 3 nm-C6OEt, which is consistent with data established for planar samples (Fig. 4).

3.3.3. Mechanical properties – nanotribological study

To achieve better characterization of modified materials, not only the physiochemistry, including wettability, but also mechanical resistance should be evaluated. Force of adhesion is an important and powerful parameter in the evaluation of functionalization process quality and depending on the chemical covalent bonding, capillary forces, van der Waals, electrostatic forces, and mostly on the adhesion [55,56].

Based on the data gathered in Table 1, it can be observed that the grafting process for both perfluorinated and fluorine-free molecules meaningfully changed the mechanical properties of the ceramics described by nanotribology. Considering the adhesion of the ZrO_2 samples, a significant diminution of that parameter was observed being in the range of 81–89% of the values for the pristine samples. The smallest values were measured for samples possessing the highest hydrophobicity level and additionally less rough surfaces, grafted with FC12

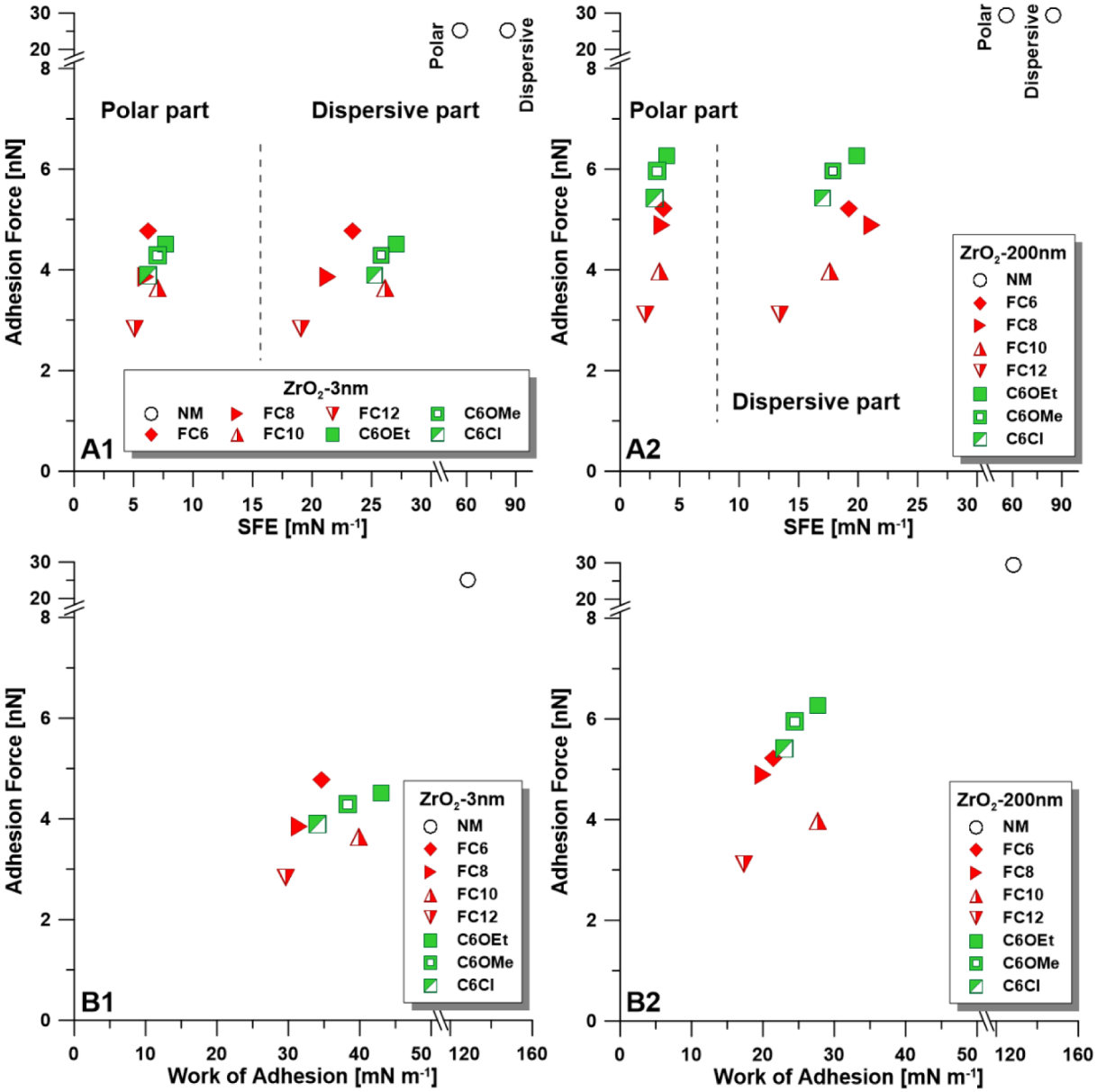

Fig. 6. The relation between adhesion force and surface free energy for 3 nm (A1) and 200 nm (A2) membranes and between work of adhesion for 3 nm (B1) and 200 nm (B2) membranes.

(Figs. 4–6). Furthermore, no influence on the membrane pore size has been observed. 3 nm-FC12 and 200 nm-FC12 were characterized by 2.84 ± 0.11 nm and 3.12 ± 0.12 nm, respectively referring to the pristine ceramics with values of F_{adh} equal to 25.21 ± 1.01 nN (3 nm-NM) and 29.47 ± 1.18 nN (200 nm-NM). Some interesting data were collected for non-fluorinated membranes. The dependency of reactive groups on the tribology was observed. The smallest value of F_{adh} was found for ZrO_2 ceramics treated with a grafting agent possessing chlorine atoms (3 nm-C6Cl 3.90 ± 0.16 nm; 200 nm-C6Cl 5.42 ± 0.22 nm) as a reactive part. These observations are in good accordance with the data presented in Figs. 3–5 and can be explained by the differences in the bonds dissociation energy [8]. Furthermore, data presented by others proved the presented statement [55,56]. Cichomski and co-workers [56] observed the decrease of F_{adh} value from 25nN to 10 nN and 22 nN after modification with 1H,1H,2H,2H-perfluorodecyltrichlorosilane and (3,3,3-trifluoropropyl) trichlorosilane molecules, respectively.

Furthermore, the Young modulus (E) and nanohardness (H) of the ZrO_2 ceramics changed after treatment with a grafting agent (Table 1). Pristine ceramics depending on the pore size were characterized by nanohardness and Young modulus equal to 2.41 ± 0.10 GPa (H for 3 nm), 118.3 ± 4.73 GPa (E for 3 nm), 2.33 ± 0.09 GPa (H for 200 nm), 111.4 ± 4.46 GPa (E for 200 nm), respectively. It was observed that hardness assessed in nanoscale increased with the intensification of the hydrophobicity of grafting molecules (i.e. utilization coating molecules with longer fluoro-carbon chains) (Table 1). This remark has important implications for the preparation of more mechanically resistant membranes. It was presented also that the presence of fluorine has a significant impact on the mechanical properties. The 3 nm and 200 nm surfaces treated with FC6 were characterized by nanohardness of 8.17 ± 0.33 GPa and 7.78 ± 0.31 GPa, accordingly. However, the values of the H parameter for ceramics treated with nonfluorinated reagents (C6OEt, C6OMe, and C6Cl) were in the range of 6.64–7.69 GPa. Moreover, taking into account the standard deviation of H, there was no difference in the nanohardness values for 3 nm and 200 nm. In the case of Young modulus, slightly smaller values were established for 200 nm membranes (Table 1).

Compared to the nanohardness also, the Young modulus values for

Table 1
Nanotribology characterization (adhesion forces, Young modulus, and nano-hardness) of 5 3 nm and 200 nm zirconia membranes.

Membrane	Adhesion force [nN]	Young modulus [GPa]	Nano hardness [GPa]
3 nm-NM	25.21 ± 1.01	118.3 ± 4.7	2.41 ± 0.10
3 nm-FC6	4.78 ± 0.19	143.5 ± 5.7	8.17 ± 0.33
3 nm-FC8	3.86 ± 0.15	147.3 ± 5.9	8.46 ± 0.34
3 nm-FC10	3.65 ± 0.15	153.0 ± 6.1	8.74 ± 0.35
3 nm-FC12	2.84 ± 0.11	158.0 ± 6.3	9.50 ± 0.38
3 nm-C6OEt	4.51 ± 0.18	127.3 ± 5.1	7.69 ± 0.31
3 nm-C6OMe	4.28 ± 0.17	120.9 ± 4.8	7.31 ± 0.29
3 nm-C6Cl	3.90 ± 0.16	110.1 ± 4.4	6.65 ± 0.27
200 nm-NM	29.47 ± 1.18	111.4 ± 4.5	2.33 ± 0.09
200 nm-FC6	5.23 ± 0.21	128.6 ± 5.2	7.78 ± 0.31
200 nm-FC8	4.90 ± 0.20	136.4 ± 5.5	7.97 ± 0.32
200 nm-FC10	3.97 ± 0.16	148.0 ± 5.9	8.35 ± 0.33
200 nm-FC12	3.12 ± 0.12	151.7 ± 6.1	8.74 ± 0.35
200 nm-C6OEt	6.27 ± 0.25	125.3 ± 5.0	7.68 ± 0.31
200 nm-C6OMe	5.96 ± 0.24	119.0 ± 4.7	7.30 ± 0.29
200 nm-C6Cl	5.42 ± 0.22	108.3 ± 4.3	6.64 ± 0.27

non-fluorinated samples were smaller from surfaces treated with perfluorinated grafting agents. The measured values of tribological parameters were in good accordance with the literature data [57]. For the fully dense material of ZrO_2, the Young modulus can be varied in the range of 105–225 GPa depending on the preparation method (e.g., spark plasma sintering or classical sintering at 1110 °C) and the presence or lack of additions, e.g., yttria [58]. The detected differences in the data of H and E in our work can be explained by the higher stiffness of the fluorocarbon chains. Furthermore, it can be associated with rotation of the backbone structure for perfluorinated molecules that is considerably smaller than for the non-fluorinated molecules, because of the smaller sizing of hydrogen atoms in comparison to fluorine ones [59]. Furthermore, the produced nanolayer of fluorine-free agents is less rigid than the one generated by the fluorinated alkylsilanes. In the case of the non-fluorinated chains, carbons can freely rotate without hindrances comparing to the fluoro-carbon molecules [55]. Similar findings were presented by Bhushan et al. [59,60]. The authors have shown that for a self-assembled monolayer with a backbone structure possessing higher stiffness, more energy is needed for the elastic distortion. The abovementioned explanation can help to understand why smaller values of H and E were found for ZrO_2 samples functionalized with fluorine-free grafting agents (Table 1) [59,60]. For a more detailed explanation, AFM profile and cross-sections of selected samples; 3 nm (Fig. 7) and 200 nm (Fig. S5) have been shown. Based on the data presented in Figs. S5 and S6, only marginal variances in size of formed cavities and in depth after nanoindentation were found.

3.4. Membrane stability

The stability of functionalized ceramic membranes with alkylsilanes and perfluoroalkylsilanes were assessed at different conditions. The chemical, as well as mechanical stability, were evaluated. Considering the data gathered in Table 2, it can be seen that all membranes were stable after 96 h of the contact with chemicals. The values of the contact angle decreased by 15%. Hexane had the strongest influence on the contact angle value. Furthermore, the membranes showed good stability after 4 h of the contact with ultrasounds (Table 2). In that case, the observed maximum reduction of CA values was equal to 10%.

The differences in the transport and separation features for the membranes after the contact with hexane and after the sonication are presented in Fig. S7. All membranes were characterized by good transport and separation properties. However, bigger impact of hexane as well as the sonication on the reduction the investigated features was found for fluorinated membranes. The value of separation factor β decreased from 59 for the 2 wt% of ethyl acetate to 51 and 38 after sonication and hexane treatment, respectively. Slight reduction in the permeate of the organic component was also observed. However, due to the diminution of contact angle from 137° (200 nm-FC6) to 117° (hexane) and 125° (sonication), respectively, an increase of water flux across the membranes was noticed. Similar tendency was observed for the ceramics grafted with non-fluorinated compounds. However, for these membranes the impact of hexane and the sonication was minor. Also the reduction of contact angles was smaller for the 200 nm-C6Cl membrane. Sample before stability test was characterized by CA = 133°. As an effect of hexane and sonication treatment the CA reduced to 122° and 109°, respectively. Therefore, it can be pointed out that the membranes possess high stability and maintain their separation performance.

3.5. Membrane separation – VOCs removal from water

3.5.1. Transport of water across the functionalized membranes

Prior to the membrane separation effectiveness, the transport properties of modified ZrO_2 ceramic membranes in contact with pure water was determined. Transport of solvent vapors (i.e., water) in the membrane distillation process can be expressed in the following way (Eqs. (11) and (12)) [61]:

$$J_{H2O} = K(p_f - p_p) \tag{11}$$

$$K = \left[\frac{1}{K_f} + \frac{1}{K_m} + \frac{1}{K_p}\right]^{-1} \tag{12}$$

where K – overall mass transfer coefficient [kg $m^{-2}s^{-1}Pa^{-1}$], p_f – partial vapor pressure of water in feed, p_p – partial vapor pressure of water in permeate; K_f – mass transfer coefficient of feed layer, K_m – mass transfer coefficient of membrane and K_p – mass transfer coefficient of permeate layer.

K parameter strongly depends on the membrane features, e.g., porosity, membrane material, pore size, surface morphology, and membrane tortuosity [62]. Even though the mass transfer coefficient K is subjected to pressure and temperature, frequently, its value is practically constant [62]. Such observation has also been found in the case of zirconia modified membranes (Table 3). The vapor pressure of water was calculated from the Bulk's equation (Eq. (13)), which is a more accurate approach than the sole Antoine's equation [63].

$$P = 0.61121 exp\left[\left(18.678 - \frac{T}{234.5}\right)\left(\frac{T}{257.14 + T}\right)\right] \tag{13}$$

where temperature (T) is in [°C], and pressure (P) is in [kPa].

Taking into account the data presented in Table 3, the slight impact of membrane pore size, and the type of grafting agents has been observed. Practically, there was no influence on the type of reactive group in non-fluorinated molecules on the transfer coefficient. This observation can be elucidated by the fact that the reactive group can be influenced only by the chemistry of the surface (Figs. 4 and 6) but not the pore size (Fig. 3B), and subsequently the transport features (J_{H2O} and K). The observed reduction of K value with an increase in the length of perfluoroalkylsilanes molecules was related to the higher hydrophobicity level and subsequently with less favorable water transport across the ceramic material. Membranes treated with FC6 possessed the highest values of the mass transfer coefficient. On the other hand, the smallest value of K observed for FC12 modification might be explained by the partial clogging of pores, particularly for the 3 nm sample for which the size of grafting molecules (≈2.2 nm) is comparable with a membrane pore size (3 nm).

3.5.2. Transport and separation features of modified membranes

All prepared membranes were tested in vacuum membrane distillation for the removal of volatile organic compounds from water. The collected results are shown in Figs. 8 and 9, S7–S13. As was presented

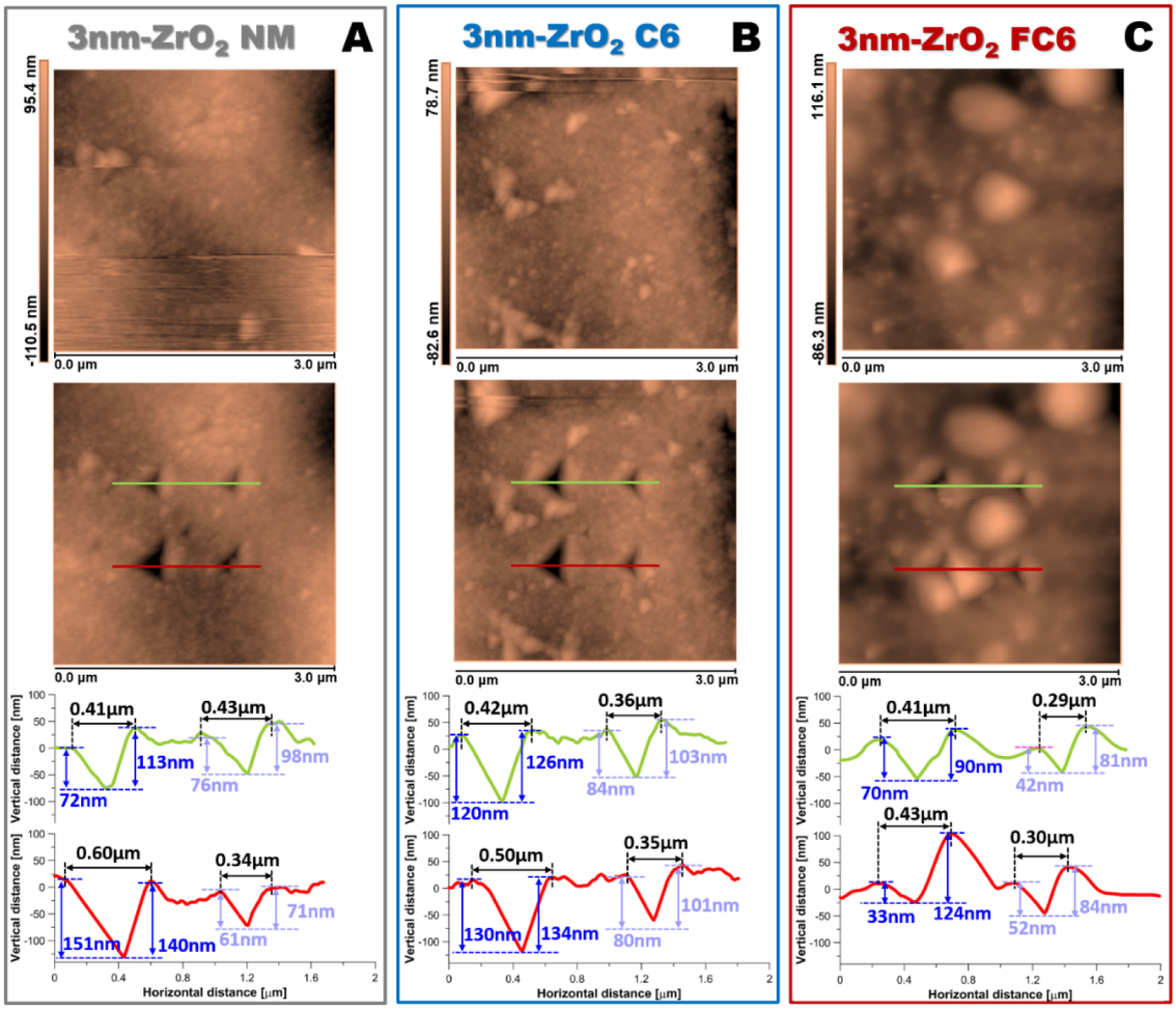

Fig. 7. Nanoindentation analysis of pristine (A) and modified 3 nm membranes with C6 (B) and FC6 (C) molecules.

previously in Fig. 4, all membrane samples were efficiently modified and possessed hydrophobic character. Furthermore, the lack of membrane wetting was supported by calculations of critical surface tension (γ_{cr}) (Fig. 4). The established values of γ_{cr} were in the range of 13.6 ± 0.4 mN m^{-1} (200 nm-FC12) and 24.2 ± 0.7 mN m^{-1} (3 nm-FC6) which means that only liquid having a value of liquid tension below 13.6 mN m^{-1} will wet these membranes. Liquid surface tensions for 3 wt% of investigated VOCs are placed between 62.8 mN m^{-1} (MTBE) and 64.0 mN m^{-1} (BuOH). The differences in membrane transport and separation efficiency are associated mostly with the pore size (3 and 200 nm). Furthermore, also the type of grafting agent influences the separation process (Fig. 8A1, 8.C1, S8.A1, S8.C1, S9.A1,

Table 2
Membrane stability in contact with various solvents and after sonication.

Membrane	CA [deg]	Membrane stability under various conditions						
		Acetone	BuOH	Chloroform	EtAc	Hexene	MTBE	Sonication
3 nm-FC6	122	113	112	109	111	104	110	114
3 nm-FC8	125	114	116	113	115	109	112	117
3 nm-FC10	117	104	106	105	107	99	104	108
3 nm-FC12	126	118	115	109	113	114	111	113
3 nm-C6OEt	114	109	107	104	107	102	104	108
3 nm-C6OMe	118	109	108	105	107	100	106	110
3 nm-C6Cl	122	114	111	105	109	110	107	109
200 nm-FC6	137	129	127	122	125	117	123	125
200 nm-FC8	128	117	115	111	114	105	111	116
200 nm-FC10	140	129	126	121	123	119	125	127
200 nm-FC12	135	123	125	121	123	111	118	124
200 nm-C6OEt	128	117	115	111	114	109	117	118
200 nm-C6OMe	132	124	122	117	120	112	118	120
200 nm-C6Cl	133	121	123	119	121	109	116	122

Table 3
Overall mass transfer coefficient for the investigated membranes.

3 nm	J_{H2O} [kg m^{-2} s^{-1}]	K [kg m^{-2} s^{-1} Pa^{-1}]	200 nm	J_{H2O} [kg m^{-2} s^{-1}]	K [kg m^{-2} s^{-1} Pa^{-1}]
FC6	5.83	$2.88 \cdot 10^{-7}$	**FC6**	6.35	$3.14 \cdot 10^{-7}$
FC8	5.17	$2.55 \cdot 10^{-7}$	**FC8**	5.72	$2.83 \cdot 10^{-7}$
FC10	4.40	$2.17 \cdot 10^{-7}$	**FC10**	5.28	$2.61 \cdot 10^{-7}$
FC12	3.52	$1.74 \cdot 10^{-7}$	**FC12**	4.99	$2.47 \cdot 10^{-7}$
C6OEt	5.72	$2.83 \cdot 10^{-7}$	**C6OEt**	6.16	$3.04 \cdot 10^{-7}$
C6OMe	5.55	$2.74 \cdot 10^{-7}$	**C6OMe**	6.07	$3.00 \cdot 10^{-7}$
C6Cl	5.38	$2.66 \cdot 10^{-7}$	**C6Cl**	5.98	$2.95 \cdot 10^{-7}$

S9.A2), particularly in the case of 3 nm membranes functionalized with fluorinated molecules. The best separation performance has been observed for water-EtAc system and the lowest one for the water-BuOH mixture (Fig. 9). These variances might be explained by the different polarity of VOCs. The values of the dielectric constant of selected VOCs were as follows: $\varepsilon_{EtAc} = 4.5 < \varepsilon_{MTBE} = 6.02 < \varepsilon_{BuOH} = 17.9 < \varepsilon_{H2O} = 80.1$ [8]. Based on the dielectric constant ε values, an improvement in separation effectiveness with the feed mixture polarity can be seen. An interesting relation was observed for the membranes modified with FC6 and its non-fluorinated analogue (C6). The β separation factors were quite similar, however owing to the better transport properties of non-fluorinated membranes related to a lower hydrophobicity level, the values of process separation index (PSI) were higher for the fluorine-free membranes (Fig. 9), respectively In the case of 200 nm membranes used for water-MTBE and water-BuOH, the enhancement of a PSI value of 21% and 39% was observed (Fig. 9). Considering only non-fluorinated samples, an increase of membrane performance expressed by PSI of 53% − 95% has been seen for 3 nm membranes and up to 53% for 200 nm when the samples treated with C6OEt and C6Cl were compared. Better transport and separation for the ceramics hydrophobized with C6Cl shows the importance of the higher reactivity of terminal groups in the grafting agent (Figs. 4 and 9).

Interestingly, for the samples modified with fluorinated coating reagents, lower separation effectiveness was detected for the highly hydrophobic surfaces (i.e., modified with FC12). An interesting observation can be pointed out for the separation features of 3 nm and 200 nm membranes modified with perfluorinated molecules. The same phenomenon was found and discussed in our earlier works focused on the functionalization of the titania ceramic membranes [8,19]. It was proved that for 3 nm membranes, the organic-nanolayer of perfluorinated compounds is active in the course of the MD process (Figs. 8, S8, S9, S4). For that reason, it was possible to distinguish the differences in McCabe-Thiele diagrams of 3 nm membranes depending on the type of modifier. Significantly higher separation ability was shown for FC6 membranes, and a gradual reduction of these properties has been observed with an increase of a number of fluorinated carbon atoms in the molecules.

Finally, the mentioned phenomenon possessed an import impact on the separation mechanism of MD that can be dependent not only on the vapor-liquid equilibrium but also controlled by the solution-diffusion mechanism through an organic brush nanolayer (modified ceramics possessed semi-dense structure). In the case of 200 nm samples, no such activity behaviour influencing transport mechanism was found. In that case of 200 nm membrane, the functionalization caused the stable hydrophobic material, but with a highly porous and open structure, comparing to 3 nm ones. Moreover, the organic nanolayer was passive in the separation, and no differences between membranes treated with various agents were observed. In can be concluded that the transport for 200 nm ceramics was controlled solely by the liquid-vapor equilibrium [8,19]. Furthermore, taking into account the β factor, different behaviour has been observed for 3 nm and 200 nm ceramics. For 200 nm the following order was found $\beta_{FC6} > \beta_{C6} > \beta_{FC8} > \beta_{FC12} > \beta_{FC10}$ for all separated VOCs systems. The explanation of that behaviour is associated with the mechanism of functionalization, as explained in Section 3.3.1.

A significant reduction in transport of organic phase as well as water was observed for all separated mixtures due to the formation of semi-dense membranes after modification of 3 nm ceramics (Figs. 8, S8, S9). The highest transport of organics was found for samples modified with C6Cl. From one side, modified ceramics possessed a hydrophobic character, however, the hydrophobicity level was not so high because of a lack of fluorine. On the other hand, C6Cl was characterized by the best grafting efficiency due to the highest reactivity out of all non-fluorinated agents. Summarizing, the chemistry of C6Cl molecules ensures very high transport and non-wetting in the course of the MD process. Finally, the transport of water across the membranes was always higher than transport of organics due to the utilization of very diluted solutions and subsequently much lower driving force of VOCs molecules (Figs. 8, S8, S9). Modified membranes were highly stable and their maintained their hydrophobicity and organic nanolayer even after durable separation process (i.e. membrane was used during the period of 1.5 year for separation of various VOCs from water). The stability of organic nanolayer was proved by FTIR and EDX (In Figs. S10 and S11).

4. Conclusions

Highly efficient ceramic separation materials for removal of hazardous VOCs (ethyl acetate, methyl-*tert*-butyl ether, and butanol) from water were generated and comprehensively characterized. Zirconia ceramic membranes with various pore sizes (3 and 200 nm) were successfully modified employing a number of reagents including perfluoroalkylsilanes and non-fluorinated molecules. The modification turned the hydrophilic character of the material into a hydrophobic one making the membranes applicable in the MD process. All membranes were resistant to water, and no wetting occurred during the application of the membranes. The wettability was discussed from theoretical and experimental points of view. The best performance was observed for the removal of EtAc, and subsequently, the effectiveness was directly related to the physico-chemistry of used VOCs (e.g., polarity). All the hydrophobized membranes were selective toward organic solvents. Transport and separation properties were referred to material, physicochemical as well as tribological properties. An interesting correlation between surface free energy and the force of adhesion was determined. The irregularity of the grafting process with FC10 molecules was explained by the difference in the mechanism of grafting and resulting differences in roughness, lower packing density, smaller level of molecular organization, and the polymerization which occurred. Moreover, depending on the membrane pore size and generation of highly porous or semi-dense hydrophobic membranes, the differences in the transport mechanism in MD were observed. For 3 nm membranes, the contribution of solution diffusion mechanism was pointed out, whereas for 3 nm and 200 nm membranes the liquid–vapor equilibrium mechanism for 200 nm membranes was held. Subsequently, different types of membrane stability, e.g., chemical, mechanical, were evaluated. All membranes were stable and maintained their hydrophobicity after treatment with various pure organic solvents as well as after exposure to sonication. The generated hydrophobic ZrO_2 membranes possessed high contact angle (140.0° ± 1.3°), low adhesive force (2.84 ± 0.11 mN m^{-1}), small hysteresis of contact angle (15°) and very good mechanical features which were highly improved after functionalization with various grafting agents.

The most important finding is the fact that the application of non-fluorinated modifiers can be more suitable for highly permeable ceramics. It was proved that the utilization of fluorine-free molecules with the highly reactive group (F6Cl) allows the generation of hydrophobic material (CA = 122° − 3 nm; 133° − 200 nm) possessing very good transport and separation properties slightly exceeding the properties of fluorinated membranes.

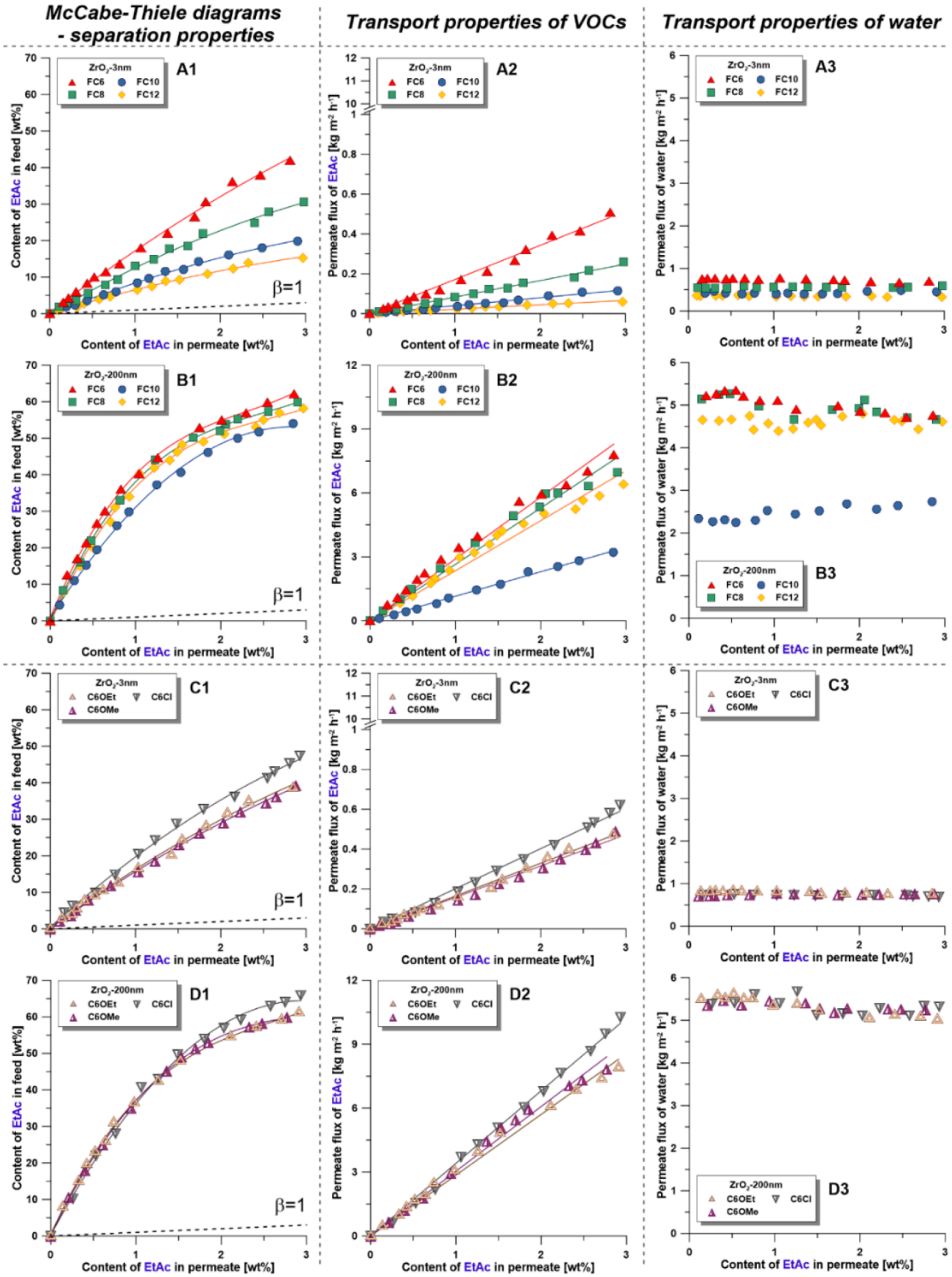

Fig. 8. Separation (1) and transport properties (2,3) in contact with a water-EtAc mixture of ceramic 3 nm (A and C) and 200 nm (B and D) membranes functionalized with fluorinated (A and B) and non-fluorinated (C and D) compounds.

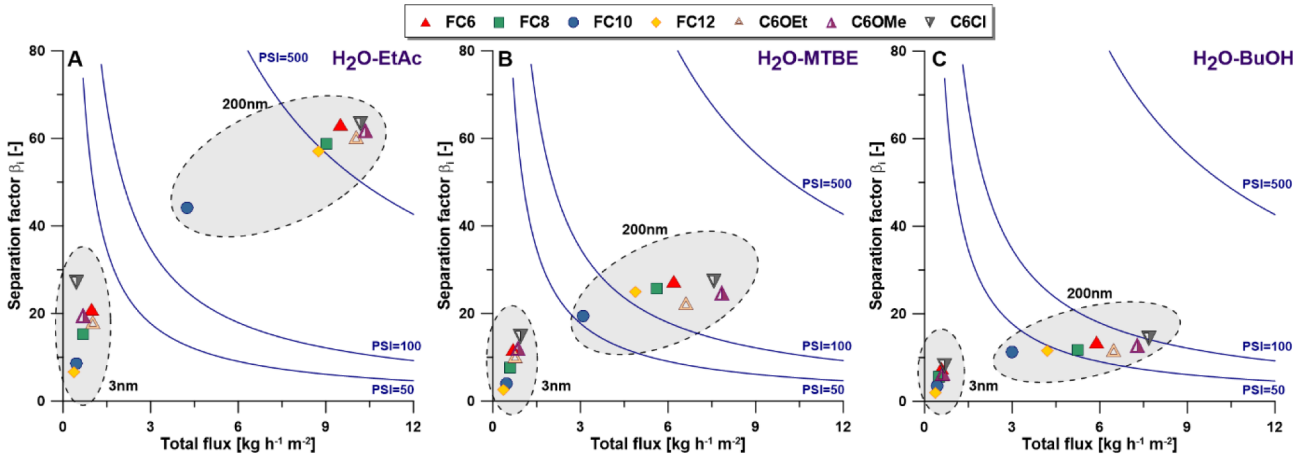

Fig. 9. Comparison of the investigated membranes performance in the separation of water-EtAc, water-MTBE, and water-BuOH mixtures; (at 1.5 wt% of VOC in feed). PSI unit is following [kg $m^{-2}h^{-1}$].

5. Future perspective

The presented results possess an important meaning in design, formation materials with tunable surface chemistry, as well as nano- or micro-architecture. Furthermore, the established data are valuable from the application point of view, e.g., lab on a chip, the fabrication of self-cleaning, and self-healing materials as well as microarrays and microsystems.

Declaration of Competing Interest

There are no conflicts of interest to declare

Acknowledgments

Special thanks are due to nLab Ltd. company (Warsaw. Poland) for the access to the goniometric equipment. Dr. Ludovic Dumée acknowledges the Australian Research Council for his ARC Discovery Early Career Research Award (DECRA) fellowship 2018 (DE180100130).

Funding: This work was supported by the 2017/26/D/ST4/00752 (Sonata 13) grant from the National Science Centre Poland. The research was supported partly by the statutory funds of Nicolaus Copernicus University in Toruń (Faculty of Chemistry. T-109).

Appendix A. Supplementary data

Supplementary data to this article can be found online at https://doi.org/10.1016/j.cej.2019.05.160.

References

[1] S.K. Hubadillah, M.H.D. Othman, T. Matsuura, M.A. Rahman, J. Jaafar, A.F. Ismail, S.Z.M. Amin, Green silica-based ceramic hollow fiber membrane for seawater desalination via direct contact membrane distillation, Sep. Purif. Technol. 205 (2018) 22–31.

[2] M. Mouiya, A. Abourriche, A. Bouazizi, A. Benhammou, Y. El Hafiane, Y. Abouliatim, L. Nibou, M. Oumam, M. Ouammou, A. Smith, H. Hannache, Flat ceramic microfiltration membrane based on natural clay and Moroccan phosphate for desalination and industrial wastewater treatment, Desalination 427 (2018) 42–50.

[3] S. Leaper, A. Abdel-Karim, T.A. Gad-Allah, P. Gorgojo, Air-gap membrane distillation as a one-step process for textile wastewater treatment, Chem. Eng. J. 360 (2019) 1330–1340.

[4] D. Woldemariam, A. Kullab, U. Fortkamp, J. Magner, H. Royen, A. Martin, Membrane distillation pilot plant trials with pharmaceutical residues and energy demand analysis, Chem. Eng. J. 306 (2016) 471–483.

[5] J.A. Prince, D. Rana, G. Singh, T. Matsuura, T. Jun Kai, T.S. Shanmugasundaram, Effect of hydrophobic surface modifying macromolecules on differently produced PVDF membranes for direct contact membrane distillation, Chem. Eng. J. 242 (2014) 387–396.

[6] Y. Fan, S. Chen, H. Zhao, Y. Liu, Distillation membrane constructed by TiO2 nanofiber followed by fluorination for excellent water desalination performance, Desalination 405 (2017) 51–58.

[7] L. García-Fernández, B. Wang, M.C. García-Payo, K. Li, M. Khayet, Morphological design of alumina hollow fiber membranes for desalination by air gap membrane distillation, Desalination 420 (2017) 226–240.

[8] J. Kujawa, S. Al-Gharabli, W. Kujawski, K. Knozowska, Molecular grafting of fluorinated and nonfluorinated alkylsiloxanes on various ceramic membrane surfaces for the removal of volatile organic compounds applying vacuum membrane distillation, ACS Appl. Mater. Interfaces 9 (2017) 6571–6590.

[9] D.H. Seo, S. Pineda, Y.C. Woo, M. Xie, A.T. Murdock, E.Y.M. Ang, Y. Jiao, M.J. Park, S.I. Lim, M. Lawn, F.F. Borghi, Z.J. Han, S. Gray, G. Millar, A. Du, H.K. Shon, T.Y. Ng, K. Ostrikov, Anti-fouling graphene-based membranes for effective water desalination, Nature Com. 9 (2018) 683.

[10] D.M. Warsinger, E.W. Tow, L.A. Maswadeh, G.B. Connors, J. Swaminathan, J.H. Lienhard V, Inorganic fouling mitigation by salinity cycling in batch reverse osmosis, Water Res. 137 (2018) 384–394.

[11] Commision Regulation The-European-Commision (EU) No 109, 2012 of 9, amending Regulation (EC) No 1907/2006 of the European Parliament and of the Council on the Registration, Evaluation, Authorisation and Restriction of Chemicals (REACH) as regards Annex XVII (CMR substances) Off. J. Eur. Union 2 2012, February 2012, 1-37.

[12] W. Lin, X. Xie, X. Wang, Y. Wang, D. Segets, J. Sun, Efficient adsorption and sustainable degradation of gaseous acetaldehyde and o-xylene using rGO-TiO2photocatalyst, Chem. Eng. J. 349 (2018) 708–718.

[13] B. Kim, Y.R. Lee, H.Y. Kim, W.S. Ahn, Adsorption of volatile organic compounds over MIL-125-NH2, Polyhedron 154 (2018) 343–349.

[14] H. Nigar, I. Julián, R. Mallada, J. Santamaría, Microwave-assisted catalytic combustion for the efficient continuous cleaning of VOC-containing air streams, Environ. Sci. Technol. 52 (2018) 5892–5901.

[15] A. Alkhudhiri, N. Darwish, N. Hilal, Membrane distillation: a comprehensive review, Desalination 287 (2012) 2–18.

[16] L.F. Dumée, S. Gray, M. Duke, K. Sears, J. Schütz, N. Finn, The role of membrane surface energy on direct contact membrane distillation performance, Desalination 323 (2013) 22–30.

[17] N. Subramanian, A. Qamar, A. Alsaadi, A. Gallo, M.G. Ridwan, J.-G. Lee, S. Pillai, S. Arunachalam, D. Anjum, F. Sharipov, N. Ghaffour, H. Mishra, Evaluating the potential of superhydrophobic nanoporous alumina membranes for direct contact membrane distillation, J. Colloid Interf. Sci. 533 (2019) 723–732.

[18] Y. Yang, Q. Liu, H. Wang, F. Ding, G. Jin, C. Li, H. Meng, Superhydrophobic modification of ceramic membranes for vacuum membrane distillation, Chin. J. Chem. Eng. 25 (2017) 1395–1401.

[19] W. Kujawski, J. Kujawa, E. Wierzbowska, S. Cerneaux, M. Bryjak, J. Kujawski, Influence of hydrophobization conditions and ceramic membranes pore size on their properties in vacuum membrane distillation of water–organic solvent mixtures, J. Membr. Sci. 499 (2016) 442–451.

[20] A. Hausmann, P. Sanciolo, T. Vasiljevic, M. Weeks, M. Duke, Integration of membrane distillation into heat paths of industrial processes, Chem. Eng. J. 211–212 (2012) 378–387.

[21] E. Karbasi, J. Karimi-Sabet, J. Mohammadi-Rovshandeh, M. Ali Moosavian, H. Ahadi, Y. Amini, Experimental and numerical study of air-gap membrane distillation (AGMD): novel AGMD module for Oxygen-18 stable isotope enrichment, Chem. Eng. J. 322 (2017) 667–678.

[22] L.D. Tijing, Y.C. Woo, M.A.H. Johir, J.-S. Choi, H.K. Shon, A novel dual-layer bicomponent electrospun nanofibrous membrane for desalination by direct contact membrane distillation, Chem. Eng. J. 256 (2014) 155–159.

[23] X. Yang, H. Pang, J. Zhang, A. Liubinas, M. Duke, Sustainable waste water deammonification by vacuum membrane distillation without pH adjustment: role of water chemistry, Chem. Eng. J. 328 (2017) 884–893.

[24] I. Das, G. De, Zirconia based superhydrophobic coatings on cotton fabrics exhibiting excellent durability for versatile use, Sci. Rep. 5 (2015) 18503.
[25] R. Das, K. Sondhi, S. Majumdar, S. Sarkar, Development of hydrophobic clay–alumina based capillary membrane for desalination of brine by membrane distillation, J. Asian Ceram. Soc. 4 (2016) 243–251.
[26] B. Khorshidi, I. Biswas, T. Ghosh, T. Thundat, M. Sadrzadeh, Robust fabrication of thin film polyamide-TiO(2) nanocomposite membranes with enhanced thermal stability and anti-biofouling propensity, Sci. Rep. 8 (2018) 784.
[27] L.M. Camacho, L. Dumée, J. Zhang, J.-D. Li, M. Duke, J. Gomez, S. Gray, Advances in membrane distillation for water desalination and purification applications, Water 5 (2013) 94.
[28] T. Liu, L. Lei, J. Gu, Y. Wang, L. Winnubst, C. Chen, C. Ye, F. Chen, Enhanced water desalination performance through hierarchically-structured ceramic membranes, J. Eur. Ceram. Soc. 37 (2017) 2431–2438.
[29] F. Wu, Y. Cao, H. Liu, X. Zhang, High-performance UiO-66-NH2 tubular membranes by zirconia-induced synthesis for desulfurization of model gasoline via pervaporation, J. Membr. Sci. 556 (2018) 54–65.
[30] J. Zhang, N. Li, D. Ng, I.A. Ike, Z. Xie, S. Gray, Depletion of VOC in wastewater by vacuum membrane distillation using a dual-layer membrane: mechanism of mass transfer and selectivity, Environ. Sci.: Water Res. Technol. 5 (2019) 119–130.
[31] D.Y. Kwok, A.W. Neumann, Contact angle measurement and contact angle interpretation, Adv. Colloid Interface Sci. 81 (1999) 167–249.
[32] W.A. Zisman, Relation of the Equilibrium Contact Angle to Liquid and Solid Constitution, Contact Angle, Wettability, and Adhesion, American Chemical Society, 1964, pp. 1–51.
[33] K.-Y. Law, H. Zhao, Determination of Solid Surface Tension by Contact, Angle, in: Surface Wetting: Characterization, Contact Angle, and Fundamentals, Springer International Publishing, Cham, 2016, pp. 135–148.
[34] A. Lecloux, J.P. Pirard, The importance of standard isotherms in the analysis of adsorption isotherms for determining the porous texture of solids, J. Colloid Interf. Sci. 70 (1979) 265–281.
[35] C. Scherdel, G. Reichenauer, M. Wiener, Relationship between pore volumes and surface areas derived from the evaluation of N2-sorption data by DR-, BET- and t-plot, Micropor. Mesopor. Mat. 132 (2010) 572–575.
[36] J. Kujawa, W. Kujawski, S. Koter, K. Jarzynka, A. Rozicka, K. Bajda, S. Cerneaux, M. Persin, A. Larbot, Membrane distillation properties of TiO_2 ceramic membranes modified by perfluoroalkylsilanes, Desalin. Water. Treat. 51 (2013) 1352–1361.
[37] J. Kujawa, S. Cerneaux, W. Kujawski, Removal of hazardous volatile organic compounds from water by vacuum pervaporation with hydrophobic ceramic membranes, J. Membr. Sci. 474 (2015) 11–19.
[38] J.E. Mu, Y.T. Shi, F. Yuan, J. Liu, Mechanochemical Behavior of BaNd2Ti4O12 Powder in Ball Milling for High κ Microwave Applications, Advances and Applications in Electroceramics II, John Wiley & Sons Inc, 2012, pp. 135–146.
[39] J.J. Bikerman, The Nature of the equilibrium spreading pressure, Kolloid. Z. Z Polym. 191 (1963) 33–35.
[40] R.J. Good, Spreading pressure and contact angle, J. Colloid Interf. Sci. 52 (1975) 308–313.
[41] J. Kujawa, S. Cerneaux, W. Kujawski, Characterization of the surface modification process of Al2O3, TiO2 and ZrO2 powders by PFAS molecules, Colloids Surf A 447 (2014) 14–22.
[42] L. Matějová, O. Šolcová, P. Schneider, Standard (master) isotherms of alumina, magnesia, titania and controlled-pore glass, Micropor. Mesopor. Mat. 107 (2008) 227–232.
[43] M. Thommes, K. Kaneko, V. Neimark Alexander, P. Olivier James, F. Rodriguez-Reinoso, J. Rouquerol, S.W. Sing Kenneth, Physisorption of gases, with special reference to the evaluation of surface area and pore size distribution (IUPAC Technical Report), Pure Appl. Chem. (2015) 1051.
[44] P. Schneider, Adsorption isotherms of microporous-mesoporous solids revisited, Appl. Catal. A 129 (1995) 157–165.
[45] M.U.M. Junaidi, C.P. Leo, A.L. Ahmad, N.A. Ahmad, Fluorocarbon functionalized SAPO-34 zeolite incorporated in asymmetric mixed matrix membranes for carbon dioxide separation in wet gases, Micropor. Mesopor. Mat. 206 (2015) 23–33.
[46] M. Psarski, G. Celichowski, E. Bystrzycka, D. Pawlak, J. Grobelny, M. Cichomski, Vapor phase deposition of fluoroalkyl trichlorosilanes on silicon and glass: influence of deposition conditions and chain length on wettability and adhesion forces, Mater. Chem. Phys. 204 (2018) 305–314.
[47] M. Shaker, E. Salahinejad, A combined criterion of surface free energy and roughness to predict the wettability of non-ideal low-energy surfaces, Prog. Org. Coat. 119 (2018) 123–126.
[48] V.H. Dalvi, P.J. Rossky, Molecular origins of fluorocarbon hydrophobicity, P. Natl. Acad. Sci. 107 (2010) 13603–13607.
[49] T.M. Miller, Atomic and molecular polarizabilities, in: D.R. Lide (Ed.), CRC Handbook of Chemistry and Physics, 96th Ed., CRC, Internet Version 2010, Boca Raton, FL, 2010, pp. 10193–10202.
[50] K.G. Nayar, D. Panchanathan, G.H. McKinley, J.H. Lienhard, Surface tension of seawater, J. Phys. Chem. Ref. Data 43 (2014) 043103.
[51] E. Lippert, The strengths of chemical bonds, Angew. Chem. 72 (1960) 602.
[52] H.Y. Erbil, Calculation of spreading pressure of water on cellulosic films from contact angle data, Turk. J. Chem. 21 (1997) 332–345.
[53] L. Gao, T.J. McCarthy, Teflon is hydrophilic comments on definitions of hydrophobic, shear versus tensile hydrophobicity, and wettability characterization, Langmuir 24 (2008) 9183–9188.
[54] A. Rana, A. Patra, M. Annamalai, A. Srivastava, S. Ghosh, K. Stoerzinger, Y.-L. Lee, S. Prakash, R.Y. Jueyuan, P.S. Goohpattader, N. Satyanarayana, K. Gopinadhan, M.M. Dykas, K. Poddar, S. Saha, T. Sarkar, B. Kumar, C.S. Bhatia, L. Giordano, Y. Shao-Horn, T. Venkatesan, Correlation of nanoscale behaviour of forces and macroscale surface wettability, Nanoscale 8 (2016) 15597–15603.
[55] B. Bhushan, M. Cichomski, E. Hoque, A. DeRose, P. Hoffmann, J. Mathieu, Nanotribological characterization of perfluoroalkylphosphonate self-assembled monolayers deposited on aluminum-coated silicon substrates, Microsyst. Technol. 12 (2006) 588–596.
[56] M. Cichomski, K. Kośla, W. Pawlak, W. Kozłowski, W. Szmaja, Stability and tribological investigations of 1H, 1H, 2H, 2H-perfluoroalkyltrichlorosilane on titania surface, Tribol. Int. 77 (2014) 1–6.
[57] M. Keshavarz, M.H. Idris, N. Ahmad, Mechanical properties of stabilized zirconia nanocrystalline EB-PVD coating evaluated by micro and nano indentation, J. Adv. Ceram. 2 (2013) 333–340.
[58] J.J.R. Rovira, E.J. Piqué, M.J. Anglada Gomila, Nanoindentation of Advanced Ceramics: Applications to ZrO_2 Materials, in: A. Tiwari, S. Natarajan (Eds.), Applied Nanoindentation in Advanced Materials, John Wiley & Sons Ltd, Oxford, UK, 2017, pp. 459–480.
[59] B. Bhushan, T. Kasai, G. Kulik, L. Barbieri, P. Hoffmann, AFM study of perfluoroalkylsilane and alkylsilane self-assembled monolayers for anti-stiction in MEMS/NEMS, Ultramicroscopy 105 (2005) 176–188.
[60] B. Bhushan, H. Liu, Nanotribological properties and mechanisms of alkylthiol and biphenyl thiol self-assembled monolayers studied by AFM, Phys. Rev B 63 (2001) 245412.
[61] C.M. Guijt, G.W. Meindersma, T. Reith, A.B.d. Haan, Air gap membrane distillation: 2. Model validation and hollow fibre module performance analysis, Sep. Purif. Technol. 43 (2005) 245–255.
[62] A.M. Alklaibi, N. Lior, Transport analysis of air-gap membrane distillation, J. Membr. Sci. 255 (2005) 239–253.
[63] J. Straub, NBS/NRC steam tables. Von L. Haar, J. S. Gallagher und G. S. Kell. Hemisphere Publishing Corp., Washington–New York–London 1984. 1. Aufl., XII, 320 S., geb., $ 34.50, Chem. Ing. Tech., 57 (1985) 812-812.